DOT/FAA/NR-91/9

Project Report
ATC-183

Analysis of the Terminal Doppler Weather Radar Algorithm for Detecting Rotation Associated with Microbursts

V. C. Coel

25 October 1991

Lincoln Laboratory
MASSACHUSETTS INSTITUTE OF TECHNOLOGY
LEXINGTON, MASSACHUSETTS

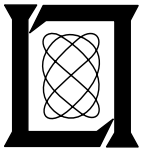

Prepared for the Federal Aviation Administration,
Washington, D.C. 20591

This document is available to the public through
the National Technical Information Service,
Springfield, VA 22161

TECHNICAL REPORT STANDARD TITLE PAGE

1. Report No.	2. Government Accession No.	3. Recipient's Catalog No.
ATC-183	DOT/FAA/NR-91/9	

4. Title and Subtitle	5. Report Date
Analysis of the Terminal Doppler Weather Radar Algorithm for Detecting Rotation Associated with Microbursts	25 October 1991
	6. Performing Organization Code
7. Author(s)	8. Performing Organization Report No.
Valerie C. Coel	ATC-183
9. Performing Organization Name and Address	10. Work Unit No. (TRAIS)
Lincoln Laboratory, MIT P.O. Box 73 Lexington, MA 02173-9108	11. Contract or Grant No. DTFA-01-89-Z-02033
12. Sponsoring Agency Name and Address	13. Type of Report and Period Covered
Department of Transportation Federal Aviation Administration Systems Research and Development Service Washington, DC 20591	Project Report
	14. Sponsoring Agency Code

15. Supplementary Notes

This report is based on studies performed at Lincoln Laboratory, a center for research operated by Massachusetts Institute of Technology. The work was sponsored by the Department of the Air Force under Contract F19628-90-C-0002.

16. Abstract

Rotating winds aloft occurring with downdrafts often are associated with microbursts, which are serious aviation hazards. The Terminal Doppler Weather Radar system detects microbursts and warns pilots of windshear events, partly by its use of rotation regions as precursors. The role of the rotation region detection algorithm in this system is described, and the improvements to it are analyzed using measured data and simulated rotation regions. The final results show a substantial overall decrease in the number of false detections generated by the algorithm due to adjustment of thresholds and additional logic, while still retaining a good probability of microburst rotation region detection (84 percent). Ideas for future enhancement are explored through techniques such as discriminant analysis and environmental wind filtering.

17. Key Words		18. Distribution Statement
azimuthal shear	parameter tuning	This document is available to the public through the National Technical Information Service, Springfield, VA 22161.
feature extraction	scoring	
algorithm performance		

19. Security Classif. (of this report)	20. Security Classif. (of this page)	21. No. of Pages	22. Price
Unclassified	Unclassified	70	

ABSTRACT

Rotating winds aloft occurring with downdrafts often are associated with microbursts, which are serious aviation hazards. The Terminal Doppler Weather Radar system detects microbursts and warns pilots of windshear events, partly by its use of rotation regions as precursors. The role of the rotation region detection algorithm in this system is described, and the improvements to it are analyzed using measured data and simulated rotation regions. The final results show a substantial overall decrease in the number of false detections generated by the algorithm due to adjustment of thresholds and additional logic, while still retaining a good probability of microburst rotation region detection (84 percent). Ideas for future enhancement are explored through techniques such as discriminant analysis and environmental wind filtering.

ACKNOWLEDGMENTS

The author wishes to thank the people whose advice and assistance has been invaluable in the preparation of this report: Leslie Mahn, for her proofreading and help with publication, Alex Jackl, for providing relief from desktop publishing nightmares, Jeff Stillson, for his discriminant analysis program and endless patience, Mark Isaminger, for the truth generation and meteorological insight, Marilyn Wolfson, for her help with background information, and Jim Evans, for his guidance.

TABLE OF CONTENTS

LIST OF ILLUSTRATIONS

Figure Page

LIST OF TABLES

1. INTRODUCTION

When a microburst occurs near an airport, an aircraft on approach or departure may experience hazardous weather conditions. A system called the Terminal Doppler Weather Radar (TDWR) has been developed to automatically detect the presence of microbursts and other wind shear phenomena and to alert air traffic controllers of potential hazards. The TDWR scans the airport area to obtain radar data both at the surface and aloft. The first phase of processing this data involves the application of several algorithms which identify two-dimensional reflectivity and velocity regions. The algorithm designed to detect regions of rotating winds aloft is the subject of this report.

The rotation algorithm was first developed in 1987, and since then it has been undergoing much testing and evaluation. Though it has been in use operationally for TDWR demonstrations and evaluations since 1987, it has been determined that further improvements were necessary to reduce the incidence of spurious rotation declarations and to provide more accurate detection of rotation regions associated with microbursts.

A detailed description of the algorithm and its role in the microburst recognition system is given, and the procedures used for improvements are discussed. The performance of the algorithm on data from three geographical regions was assessed, and the results were analyzed and presented here, along with an explanation of the technique of performance evaluation. The outcome of experimentation with simulated data is included as well. Finally, a set of conclusions are drawn, and suggestions for future enhancements are also provided.

2. BACKGROUND

2.1 BRIEF OVERVIEWS

2.1.1 Rotation in the Atmosphere

In a vertically sheared environment, the presence of various instabilities in the atmosphere, such as an updrafts and downdrafts, can cause a region of air to rotate. In theory, as shown in Figure 1, one way this can happen is that the vertical shear causes a rolling vortex, and when its middle is forced upward by an updraft, the bisected cylinder forms *two* regions, now rotating in opposite directions, in which the axes of rotation are perpendicular to the surface. In a storm cell, updrafts are often accompanied by downdrafts. The downdraft is usually due to a descending reflectivity core (precipitative loading), or water phase changes, such as melting and evaporation. In response to an accelerating downdraft, the regions becomes elongated, and the radius of the rotating region decreases while its axis lengthens. Because of the conservation of angular momentum, the region will rotate even faster.

The aloft storm structure of a surface–outflow–producing microburst often contains upper–level divergence, a descending reflectivity core, mid–level convergence, and *rotation* in the vicinity of the downdraft, as shown in Figure 2. In fact, 78 percent of those microbursts studied in Denver, 1988 had rotation regions associated with them. [1] Since these characteristics, or features, exist often several minutes before the divergent outflow at the surface, their presence can be used to enhance detection and prediction of microbursts.

2.1.2 The Microburst Recognition Algorithm

Initially, the microburst algorithm used by TDWR detected surface outflow using only surface velocity data. Subsequently, information was incorporated to deal with the features aloft mentioned above. The current TDWR algorithm employs a set of algorithms which together comprise three processing modules: feature extraction, vertical integration, and microburst recognition. [2] The feature extraction algorithms identify regions of convergence, reflectivity cells, storm cells, reflectivity cores, upper–level divergence, and rotation. These regions are then associated into three–dimensional structures during the vertical integration phase. In combination with the surface outflow information, and in accordance with a complex rule set, the structures lead to the generation of microburst alarms. These features aloft aid the time/space correlated surface features in the timely detection of low–altitude windshear by allowing an alert to be issued while the divergent signature at the surface is still weak. [3]

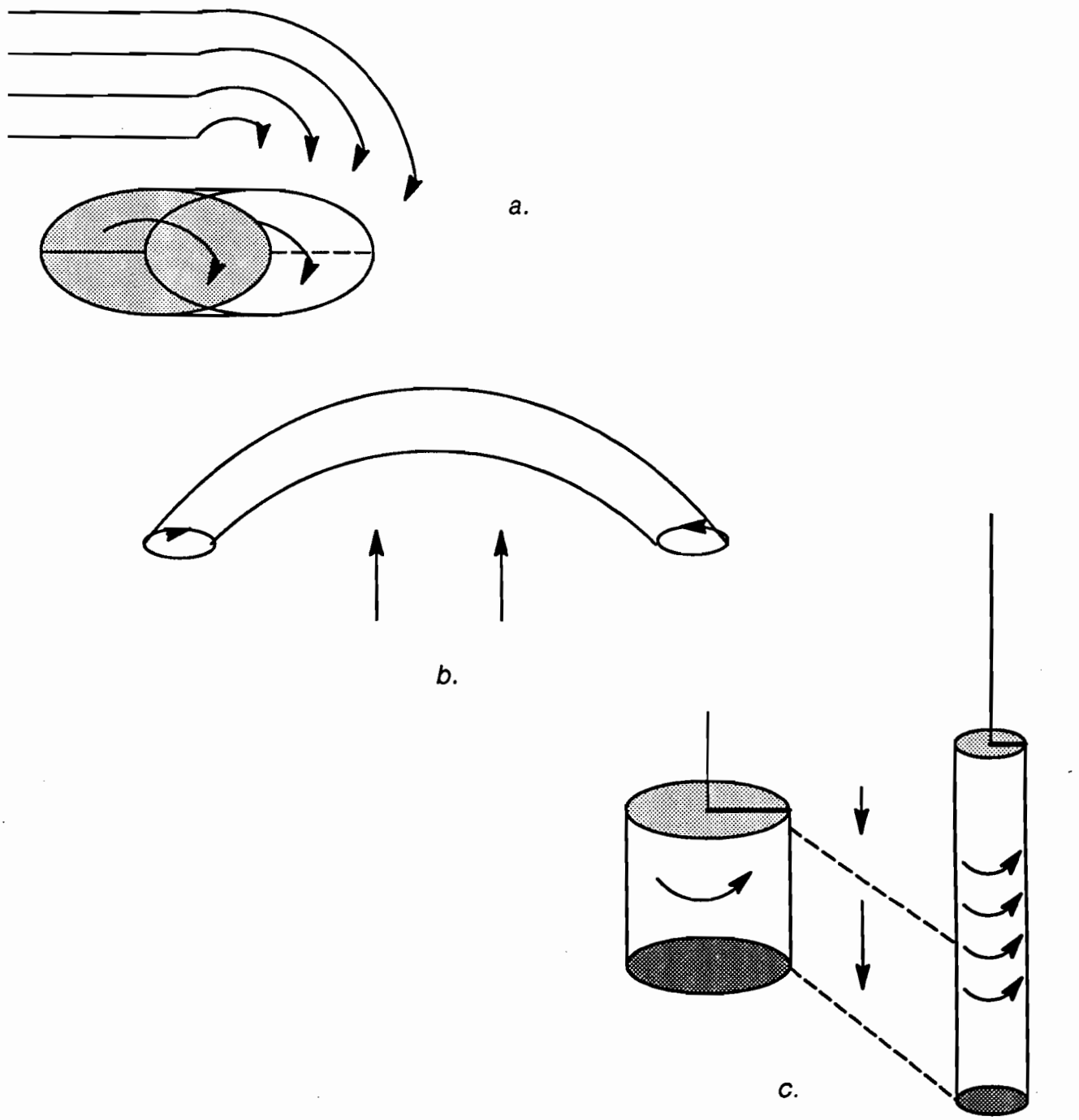

Figure 1. How Rotation Can Occur in the Atmosphere

Vertical shear causes a rolling vortex [a], and when its middle is forced upward, the bisected cylinder forms two regions, rotating in opposite directions[b], in which the axes of rotation are now perpendicular to the surface. In a storm cell, updrafts are often accompanied by downdrafts. The downdraft is usually due to a descending reflectivity core (precipitative loading), or water phase changes, such as melting and evaporation. In response to an accelerating downdraft, the radius of the rotating region decreases while its axis lengthens [c]. Because of the conservation of angular momentum, the region will rotate even faster.

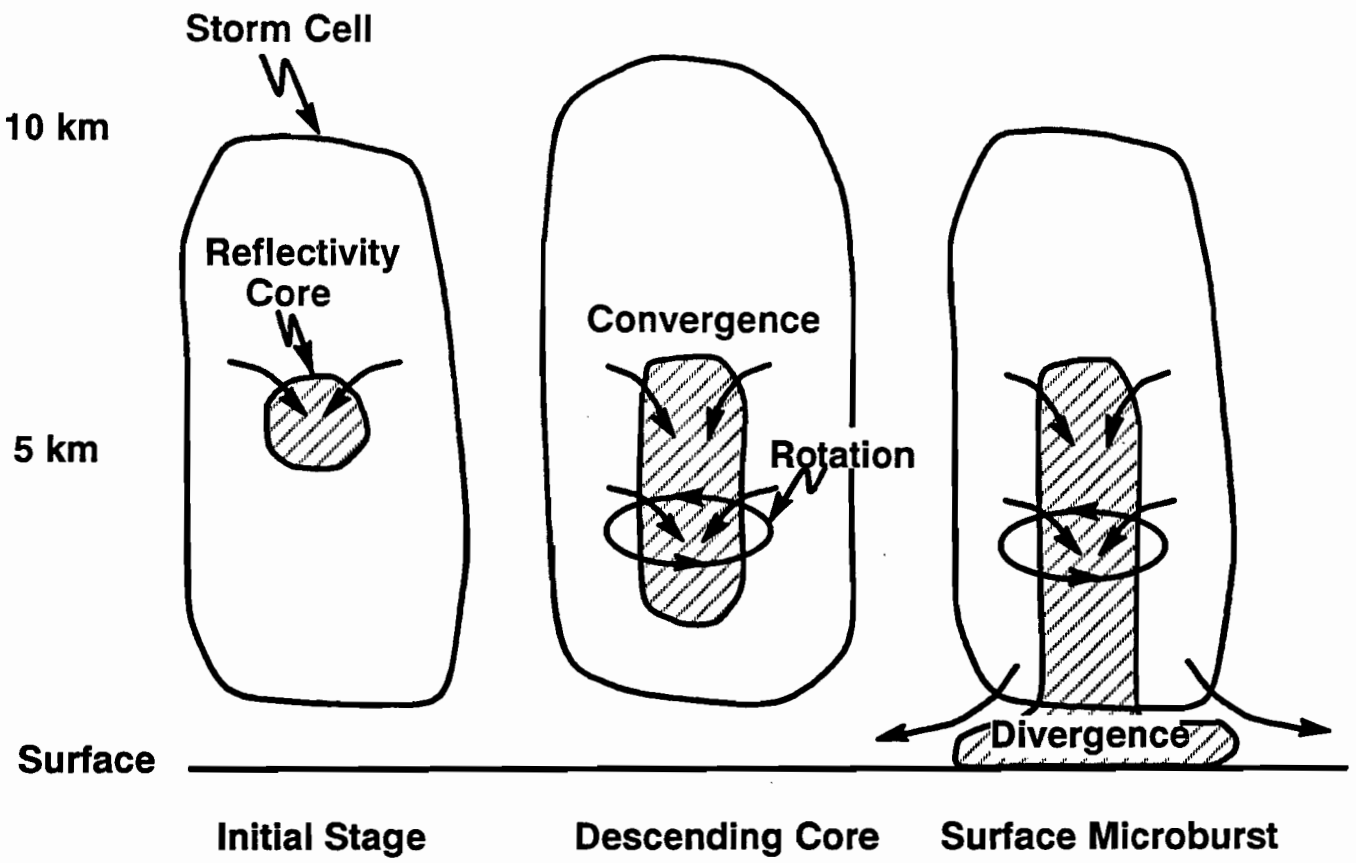

Figure 2. Storm Evolution

This figure illustrates the model of the use of features aloft as microburst precursors. As the reflective core lengthens and descends within a storm cell, convergence and rotation may be occurring aloft. In this model, the existence of these features may point to a subsequent divergent outflow at the surface.

2.1.3 The Scan Strategy

The TDWR system detects microbursts using images collected from a single Doppler radar. The beamwidth of the radar is 0.5 degrees and has a 1 degree coherent integration interval angle. Products acquired from the radar include velocity, reflectivity, signal–to–noise ratio, and spectrum width. The pulse repetition frequency (PRF) of the radar is variable in order to offset the effects of range obscuration, [4] though scans whose PRF are below 700 hz are not used by the feature extraction algorithms.

Originally, only surface scans were utilized for microburst detection, but when the importance of features aloft was recognized, it became necessary to collect data at various higher elevations. When the radar site was in Huntsville in 1986, scans were 1 degree in elevation apart, starting at 0.0 degrees and ending at 15.0 degrees, and the scans were made approximately every 10–13 seconds. The scanning sector was about 115 to 120 degrees wide. In Denver and Kansas City, surface scans were done at one–minute time intervals, and between those were five or six scans aloft at roughly equally spaced elevations, up to 40 degrees, so as to provide fairly dense coverage (no gaps greater than 1 km in height) up to an altitude of at least 6 km. This strategy allows for the same elevation to be scanned about every 2.5 minutes. [5]

3. DESCRIPTION OF THE ROTATION ALGORITHM

3.1 GENERAL DESCRIPTION OF BASE VERSION 1.4

The algorithm is based loosely on a pattern recognition algorithm developed for azimuthal shear in mesocyclones. [6] The rotation algorithm identifies, in real time, regions of cyclonic and anti-cyclonic rotation by first searching radar image data for runs of azimuthal shear. These runs, or **shear segments**, are then associated together by range and by azimuth into regions. The output of the algorithm is a set of **bounding boxes**, which are axis-aligned and enclose the x-y (cartesian coordinate) extents of the region. A flow diagram illustrating this process is shown in Figure 3.

The use of a single Doppler radar allows for only the radial component of wind velocities to be sensed, and therefore the identification of azimuthal shear can only imply a rotating wind field. This situation is illustrated in Figure 4a. Here, the solid curves are isodops representing velocities moving away from the radar, whereas the dashed lines indicate velocities moving toward the radar. The region depicted is an idealization of a large-scale vortex, [7] and results in the signature in Figure 4b. An actual radar image is given in Figure 5, in which rotation regions are indicated by red circles.

3.2 DETAILED DESCRIPTION OF BASE VERSION 1.4

3.2.1 Preliminary Processing

Input to the algorithm is polar radar data, which has been pre-processed with velocity de-aliasing and signal-to-noise thresholding, using a set of adjustable parameters. The data, in the form of radial velocity vectors, is read in by the algorithm. The first radial is buffered, and various preliminary calculations are performed. For example, these include the specification of the processing interval. This is the calculation of the range over which the algorithm will process data, taking the elevation of the scan into account, and given that we are only concerned with data lying between 1 and 6 km AGL in altitude and no further than 35 km in range from the radar.

3.2.2 Starting Segments

As soon as two radials have been read in, the search for both cyclonic and anti-cyclonic azimuthal shear begins. The velocity values within the two radials are compared at corresponding range gates. If the absolute value of the difference between the velocities in the two radials is greater than **vel_thresh**, a threshold currently set to 0, then a **shear segment** is started. In other words, the starting point of a shear segment is established when a velocity value is either monotonically increasing or decreasing with respect to the velocity azimuthally adjacent to it in the scan. The direction of the velocity change is called the **tendency**.

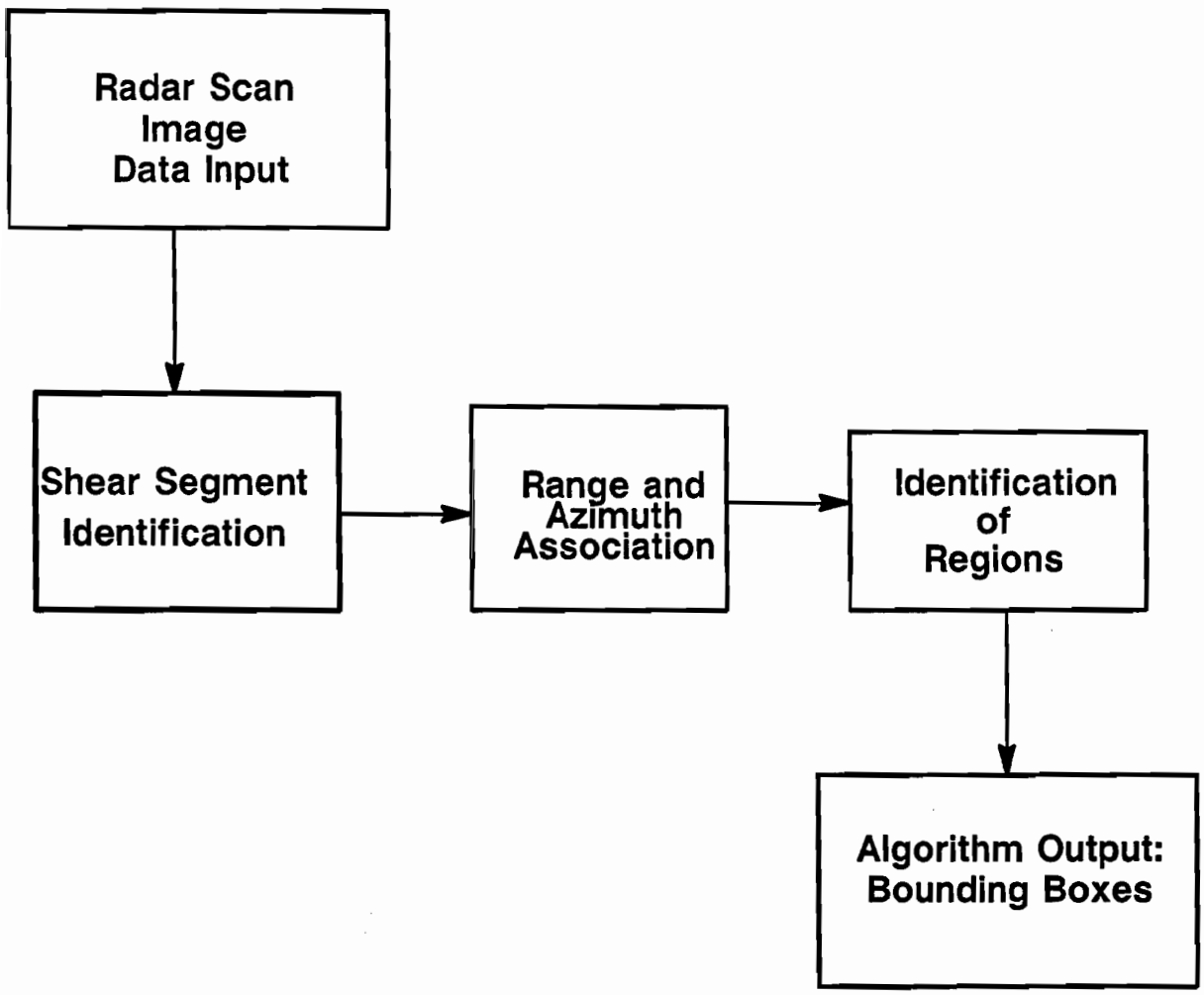

Figure 3. Algorithmic Process Flow

The rotation algorithm identifies, in real time, regions of cyclonic and anti-cyclonic rotation by first searching radar image data for runs of azimuthal shear. These runs, or **shear segments**, *are then associated spatially by range and azimuth into regions. The output of the algorithm is a set of* **bounding boxes**, *which are axis-aligned and enclose the x-y (cartesian coordinate) extents of the region.*

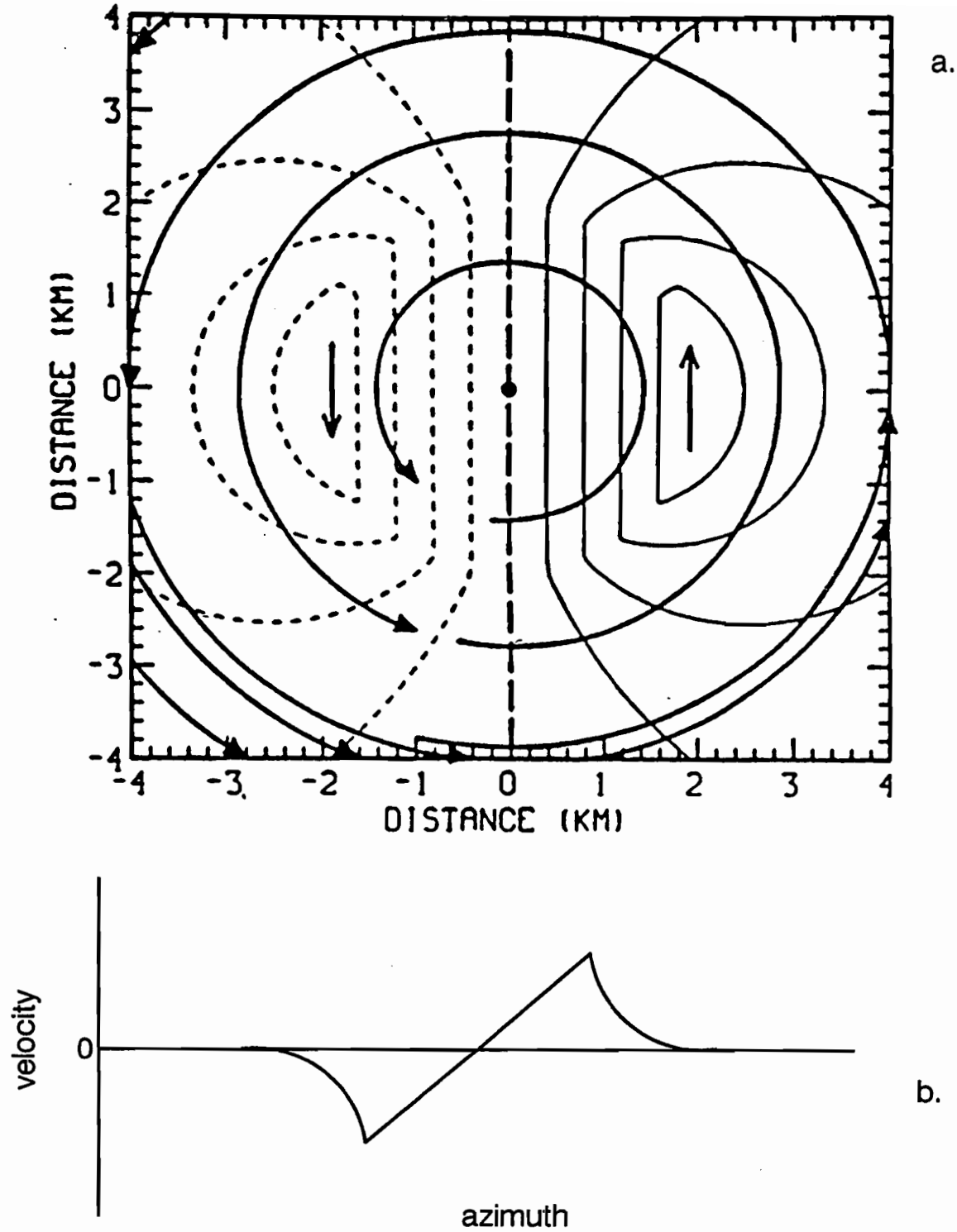

Figure 4. Rotation as Observed by Single Doppler

The use of a single Doppler radar allows for only the radial component of wind velocities to be sensed, and therefore azimuthal shear can only imply a rotating wind field. This situation is illustrated in Figure 4a. Here, the solid curves are isodops for representing velocities moving away from the radar, whereas the dashed lines are the velocities moving toward the radar. This is an idealization of a large-scale vortex, [7] and results in a signature such as that in depicted in Figure 4b.

3.2.3 Continuing Segments

To process the next radial of radar data, its velocities are now compared to those in the previous radial. For those range gates where shear segments have already been started, the decision now is whether to add another point to the segment. If the velocity at this point continues to change in the same direction as it had been (that is, the tendency remains the same), the segment is allowed to continue.

3.2.4 Ending Segments

While building a shear segment, if the tendency changes, then the shear segment is ended. The completed shear segment is now subjected to a number of tests, which will further determine if it should be retained.

3.2.5 Validating Segments

Each shear segment must have a velocity difference between its endpoints of 5 m/s for cyclonic rotation (or -5 m/s for anti-cyclonic rotation). It must have the minimum length restricted by **min_seg_len**, currently set to 1 km, but the shear segment can be no more than 5 km long. If it also spans 3 degrees in azimuth, it is retained, and the shear segment will pass to the next phase of processing.

3.2.6 Merging into Regions

All of the segments found on the scan are collected and separated in cyclonic and anti-cyclonic groups. Each of the segments in these groups are compared to all the others in that group to see if they correlate spatially. In order to do this, the two segments being compared may be no more than 1000 meters apart in range, and they must overlap in azimuth. These two thresholds are called **range_thr** and **az_thr**, respectively. If the two segments satisfy these criteria, then they are *merged*, or considered to be part of the same *region*. The segments themselves remain as separate entities, but now together they denote a region.

3.2.7 Output of Valid Regions

When all possible regions have been formed from the shear segments, attributes such as centroid location and average shear are calculated. Further testing against thresholds is performed: the maximum velocity difference in the region must be greater than or equal to the **deltav** threshold, currently 10 m/s, its centroid must lie no farther than 35 km in range, and it must have a minimum area of 1 sq-km, corresponding to **area_thr**, while being no more than 15 sq-km in area. The velocity threshold was chosen to be 10 m/s [8] because it was the threshold used in a previous analysis [9] and because a similar radial velocity associated with a microburst is considered also to be hazardous. Those regions satisfying these criteria become the final output of the algorithm.

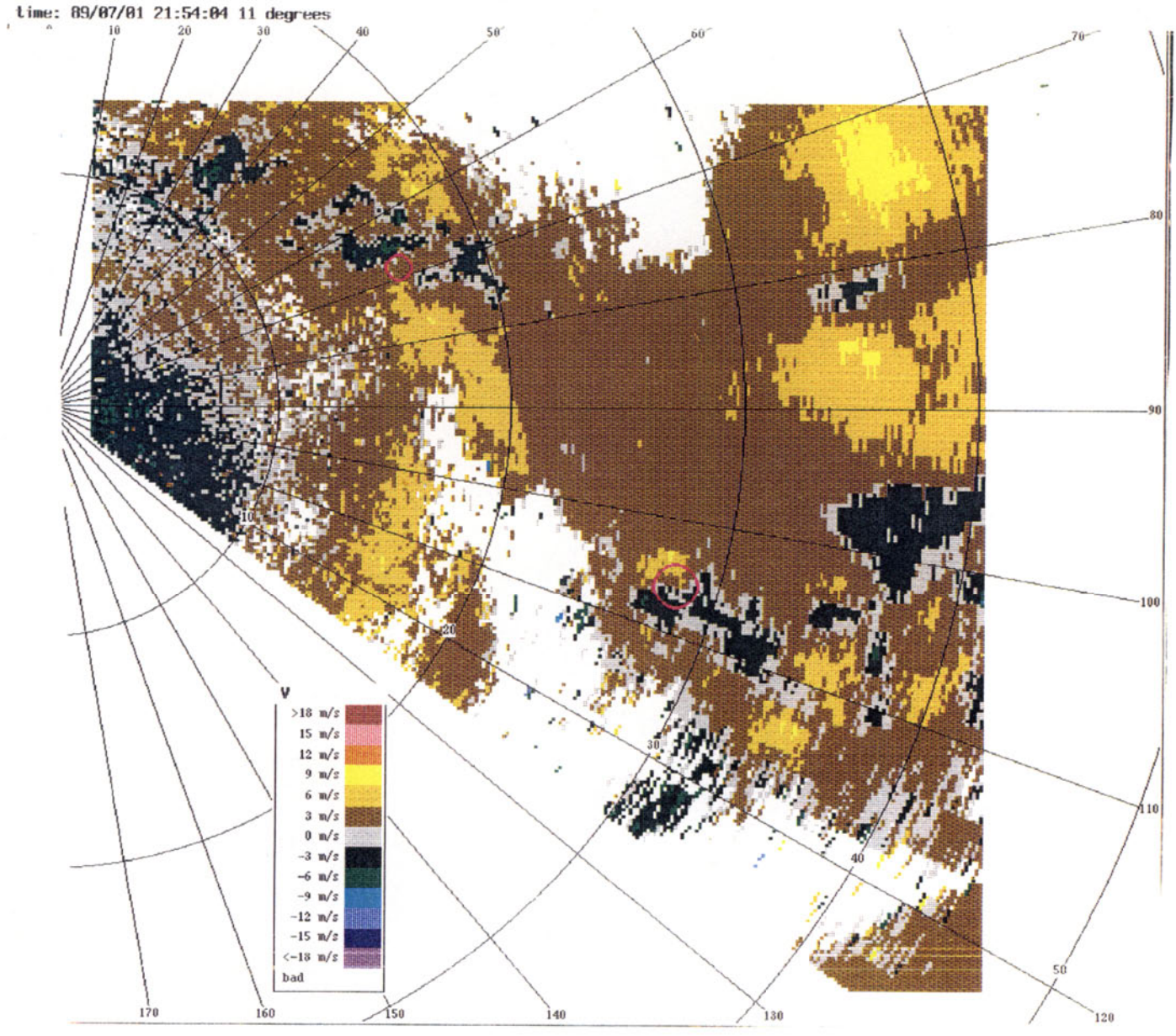

Figure 5. TDWR Image, Showing Rotation Region

This scan is from the radar site at Kansas City, on July 1, 1989 at 21:54:04 UT. The elevation of the scan is 11 degrees, range rings are 10 km apart, and azimuth lines are 10 degrees apart. Colors are denoted as in the legend, indicating m/s. The red circles are rotation regions identified by a human expert. These two regions were the only ones on this scan to meet the various truthing criteria of velocity differential, area, range, and association with a microburst-producing storm cell. Any other azimuthal shear that may be observed here is considered spurious insofar as microburst detection is concerned.

4. IMPROVEMENT AND EVALUATION PROCEDURE

4.1 OBJECTIVES

The approach taken involved a preliminary evaluation, which led to improvements and testing, and then a final evaluation. The motivations for making improvements to the algorithm were numerous. First, according to the preliminary evaluation, it appeared most important to decrease the very high probability of false detections (PFD). At the same time, it was desirable to increase the probability of detection (POD). It was of somewhat secondary importance to decrease the ratio of the total number of detections (whether ultimately correct or incorrect) to the total number of truth observations (the DTR, or the detections–to–truth–ratio). These are the basic aims, though the particular values required for the POD and PFD are unspecified at present.

It is typically the issue that a valid microburst rotation region will give rise to two regions of azimuthal shear, as illustrated in Figure 4b. However, it does complicate overall TDWR region association if more than two azimuthal shear regions are detected for a given truth region. This makes it desirable to reduce the number of detected regions in relation to the number of truth observations, the DTR.

The task of improving an algorithm can involve two types of changes: logic changes and parameter tuning. The logic changes represent the infusion of new ideas into the algorithm processing, involving changes in the intrinsic design, whereas the parameter tuning implies site adaptation parameter changes that can be made without modifying the TDWR basic software. Both of these techniques were employed in improving the performance of the rotation algorithm.

4.2 OVERALL TESTING STRATEGY

The approach taken for this study was to make logic changes and parameter tuning on two types of data sets, one small and one large. First, a small set of data would be gathered and tests would be performed on it to aid in determining the characteristics of the final version of the algorithm. Then, the revised algorithm would be run on the large data set in order to obtain statistically significant performance scoring. In this report, the small set will be referred to as "test data," and the large set will be called "case data."

4.3 DESCRIPTION OF DATA SETS

4.3.1 Test Data

A test data set was used mainly for practical reasons, given the length of time which would be needed to run the algorithm and the number of permutations of the parameter set. However, there is a difficulty inherent in the task of finding representative data, then

drawing global conclusions based on it. There is no such thing as a perfect weather model for a given geographical region. The methodology used to obtain a test data set was as follows: select case dates containing microburst events from three geographical regions where the radar has been situated. These events should be typical for their geographic regions. Then select individual scans from these events where the baseline algorithm's performance category was:

- miss -- a failure to detect
- hit -- a successful detection
- false -- a spurious detection

These performance categories will be explained in more detail in Chapter 5. Table 1 below relates to Figure 6 as follows: for each group of scans in the table, the site from which data was taken is shown along with the issue the scans were chosen to represent, i.e., why those particular scans were selected for test purposes.

Table 1.

Scan Information

SCANS	SITE	ISSUE
1-6	Kansas City	False
7-9	Denver	Miss
10-12	Huntsville	Hit
13-20	Kansas City	Miss

Tape Translated on 06/01/90
Project FLOWS

Radar FL-2 Beam 0.94 deg Polar horizontal Freq 2845MHz Pulse 0.650 micsec

Scan no. 1	prf	963	Time	06:54:56	to	06:55:00	AZ	2.5 to 127.5	EL	4.5	Dir +	Radials 126
2		943		06:57:30	to	06:57:35		128.5 to 2.5		4.5	-	127
3		967		06:59:58	to	07:00:03		3.5 to 127.5		4.5	+	125
4		963		07:10:01	to	07:10:06		2.5 to 127.5		4.5	+	126
5		727		09:06:01	to	09:06:06		23.5 to 147.5		4.5	+	125
6		708		09:18:24	to	09:18:38		149.5 to 152.5		2.1	-	358
7		708		23:06:03	to	23:06:09		280.0 to 39.7		15.6	+	162
8		708		23:06:10	to	23:06:17		40.0 to 280.3		18.6	-	173
9		708		23:06:18	to	23:06:24		280.0 to 39.7		21.9	+	170
10		900		19:03:15	to	19:03:25		269.8 to 152.9		9.0	-	121
11		1200		21:59:57	to	22:00:10		140.0 to 350.0		10.0	-	152
12		900		22:01:01	to	22:01:14		140.0 to 349.7		9.0	-	148
13		797		21:53:36	to	21:53:41		127.5 to 2.5		2.2	-	126
14		797		21:53:43	to	21:53:48		2.5 to 127.5		4.5	+	126
15		797		21:53:50	to	21:53:55		125.5 to 2.5		6.7	-	124
16		1220		21:53:57	to	21:54:02		2.5 to 127.5		8.8	+	126
17		1220		21:54:04	to	21:54:09		125.5 to 2.5		11.0	-	124
18		1220		21:54:11	to	21:54:16		1.5 to 127.5		13.1	+	127
19		707		09:28:29	to	09:28:44		149.5 to 151.5		2.1	-	359
20		1220		09:30:40	to	09:30:45		24.5 to 148.5		39.9	+	125

Figure 6. List of Test Scans

The above lists information about the scans used in the test data set. The scan number, the PRF used in hz, the scan time, the azimuths (in degrees) covered in the scanning sector, the elevation in degrees, the direction of the scan (+: clockwise, -: counter-clockwise), and the number of radials in the scan.

4.3.2 Case Data

The cases chosen for this data base represent a diversity of meteorological conditions. Weather in Kansas City, MO, July 30, 1989 was characterized by large-scale hail- generating thunderstorms with high reflectivities. The cells which developed in Huntsville, AL on July 25, 1986 and in Kansas City, MO on July 1st, 1989 were isolated air mass thundershowers with moderate to high reflectivities, while the microbursts in Denver, CO on September 2, 1987 were classified as dry due to the lower reflectivities. [8]

In this data set, there were 26 microburst events which were determined by an experienced radar meteorologist to have rotation precursors.

4.4 CHANGING THE ALGORITHM

4.4.1 Logic Improvements

A number of image processing techniques were tried, but in most cases performance was not improved, and in some cases performance was worse. Among the techniques used was a three-radial buffer as an implementation of a sliding window to calculate average velocity points, which was an attempt at noise filtering. This technique differed from that described in sections 3.2.2 and 3.2.3 in that the velocities being compared were not those belonging to successive radials. Instead, the **tendency** computation described section 3.2.2 was performed with radials 1 and 3, radials 2 and 4, and so on, in order to help decrease the algorithm's susceptibility to noise and spurious events. The technique was implemented as a substitution of the original **tendency** computation, with the existing thresholds being applied subsequently. The technique was not being used as a true filter, whereby it would pre-process the raw data before any velocity calculations were performed. Since the noise inherent in the data was not uniform, the use of this technique, in combination with the existing logic of the algorithm, caused a major drop in detection capability. In retrospect, a more effective way to use this technique would have been to apply a smoothing filter first.

The logic change that proved successful, however, was the incorporation of the *shear validation test* into the base version, and this produced Version 1.5. The purpose of the test was to keep segments from growing too long, which would happen frequently. If segments were allowed to include regions of very weak shear, the total area of a potential rotation region would exceed the maximum area threshold, causing it to be eliminated from the final output. Furthermore, segments that had become too long would be invalidated on the basis of their length, which could also cause the algorithm to miss a detection.

Though the shear validation test could be used for decreasing the number of algorithm misses, it could also help eliminate a number of false detections. By restricting the segments that were retained to have a higher overall shear value, the resulting regions detected are more likely to be physically meaningful. A higher azimuthal shear often indicates a stronger

downdraft, which in turn can lead to a more intense surface outflow. Therefore, this would help reduce the incidence of false detections.

The shear validation test works as follows: Assume that the first two radials of data have been received. Segments are started as in Version 1.4 (see section 3.2.2), but now the shear between the two points of the segment is calculated and saved for later comparisons. When the next radial of radar data is processed, its velocities are now compared to those in the previous radial, as before. For those range gates where segments have already been started, and if the **tendency** computation indicates it, the decision now is whether to add another point to the segment. In order to make this determination, the shear between the candidate point and the segment starting point is calculated and compared to the saved shear value. If, by adding this point to the segment the shear has not dropped more than x%, where x is **shear_drop**, a threshold currently set to 80, then the segment is allowed to continue, while the saved shear shear value is updated.

This concept of this test is represented graphically in Figure 7. The shear segment is started at point **a** and the shear is recorded at point **b**, as shown connected by the solid line. Though the velocity differential between azimuths drops with point **c**, the shear measured at that point passes the threshold and the current segment is now shown as a dashed line. The segment continues to **d**, as shown by the bold line. However, at point **e**, even though the velocity is still increasing, the shear drops too low, and the segment is ended. Without the use of this technique, the segment would have continued on through point **f** as indicated by the dotted lines.

The effectiveness of this technique was evaluated by designing into it a threshold that could be externally varied along with the other parameters for the algorithm. This setting of this threshold, **shear_drop**, allowed the shear validation test to range from being completely disabled to being very restrictive, and the usefulness of the test could be determined quantitatively.

4.4.2 Parameter Optimization

Optimization was accomplished by varying five parameters:

a. **shear_drop** — The fraction by which the current shear of a segment is allowed to drop and still continue the segment growth.

b. **range_thr** — A variable whose value determines the maximum distance between two candidate shear segments in order that they be considered as part of the same region.

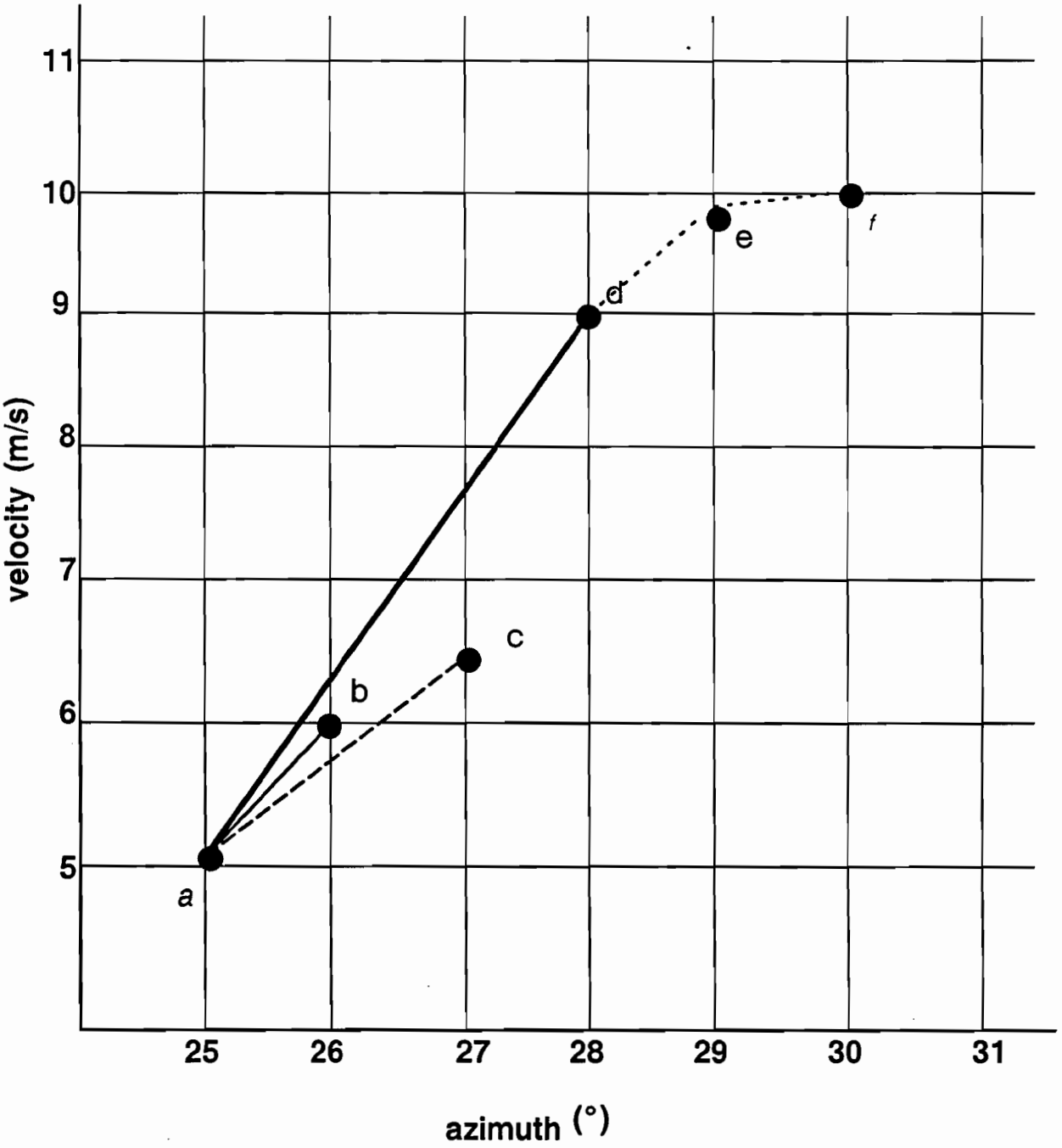

Figure 7. Shear Validation Test

Each ● represents a velocity data point. The shear segment is started at point **a** *and the shear is recorded at point* **b**, *as shown connected by the solid line. Though the velocity differential between azimuths drops with point* **c**, *the shear measured at that point passes the threshold and the current segment is now shown as a dashed line. The segment continues to* **d**, *as shown by the bold line. However, at point* **e**, *even though the velocity is still increasing, the shear drops too low, and the segment is ended. Without the use of this technique, the segment would have continued on through point* **f** *as indicated by the dotted lines. The velocity values are representational and do not conform to the algorithm thresholds.*

c. **area_thr** -- The minimum area required for a valid output region.

d. **az_thr** --The amount by which the two angular arcs represented by segments must overlap. A negative number for this parameter implies the size of a gap instead of overlap.

e. **min_seg_len** -- The minimum length of a valid shear segment.

These parameters fall into three categories: segment growing, segment association, and region validation. These represent the main functions of the algorithm and can have a potentially significant effect on its performance. It was reasonable that if the criteria for segment growing was made more restrictive, then the association step should be more lenient in order to offset the possibility of missing detections. It was not so clear, however, what would be the effect of changing **area_thr**, since its value is based on the meteorological characteristics of actual rotation regions.

The values chosen for the parameters tended to be somewhat empirical in nature, though there was an overall scheme to which the testing adhered: variables were to be changed, when possible, only one at a time in order to insure independent evaluation of the performance. After each change, the current POD and PFD were calculated. As long as the POD continued to increase and the PFD continued to decrease as a result of this change, the variable was increased in the same direction until the performance worsened. At that point, the variable was regressed to the last value that produced a positive result.

This procedure was continued for each of the five parameters until results degraded or testing became impractical. The parameter settings for thirteen of the most significant test runs are shown in Table 2. The last set of satisfactory results determined the version to be run using the case data to produce the final performance scores.

Table 2.

Parameter List: Values of the Parameters Used for Thirteen Distinct Tests of the Algorithm

	Values for each test												
Parameter	1	2	3	4	5	6	7	8	9	10	11	12	13
shear_drop*	0	0.4	0.6	0.8	0.8	0.8	0.8	0.8	0.8	0.8	0.8	0.8	0.8
range_thr (m)	1000	1000	1000	1000	500	500	500	500	500	500	240	240	240
area_thr (sq-km)	1	1	1	1	1	2	1.5	1.5	2	2	1	1.5	1
az_thr (deg)	0	0	0	0	0	0	0	-1.3	-1.3	-2.3	-2.3	-2.3	-2.3
min_seg_len (km)	1	1	1	1	1	1	1	1	1	1	1	1	0.5

*a multiplier having no units

5. SCORING PROCEDURE

Scoring is the procedure of systematically comparing algorithm output, called *bounding boxes*, to that of a human expert operating with the same set of data. The observations of the expert are called *ground truth*, or simply, "truth," and the algorithm was scored for only those rotation events within a case date where truth was available. In order to make the comparison of bounding boxes and truth, it is important that there be a consistent set of rules governing the method of declaring hits, misses and false detections. In the following discussions, the terms *detection* and *region* will be used interchangeably, according to context, in order to refer to algorithm output.

5.1 THE SCORING PROGRAM

Consistency in scoring is maintained through the use of an automatic scoring program called *ASP*. As its input, this program uses a database containing the algorithm bounding boxes and a set of truth generated for the same data. The program compares all the detected regions on a scan with all the truth on the same scan and produces a set of statistics which quantify the algorithm's ability to detect rotation regions relative to the criteria used.

5.1.1 Temporal/Spatial Criteria

If a region is within 2 km in distance from a truth observation on the same scan, *ASP* declares this a successful detection, called a *hit*, and the region and truth are said to *overlap*. An illustration of this relationship is shown in Figure 8. The scoring program also compares the regions on a scan with the truth present on previous and future scans. This type of comparison provides information on timeliness and identifies a detection that is considered to be *early* or *late*. If a region existing on the current scan overlaps truth that occurs no more than two scans or two minutes later (whichever is later), then this detection is considered *early*. Likewise, if the truth overlapping this region instead occurred two scans or two minutes earlier, then this is considered to be a *late* detection. Note that this is a two-dimensional comparison and neglects the elevations of successive scans, which are determined by the particular scanning strategy being used (see Section 2.1.3). If no correlation with truth can be found within the above criteria, then the detection is declared *false*.

The results of these comparisons are given from two points of view: regions that hit/do not hit truth, and truth that hits/does not hit regions, which therefore indicates false detections, hits and misses. The rotation algorithm can conceivably generate many regions within the vicinity of a single truth observation. In this case, the truth is considered as being hit once, and each of the regions is regarded as hitting truth. Therefore, the number of region hits may be greater than the number of truth hits. The case of multiple and single regions hitting truth are illustrated in Figure 8.

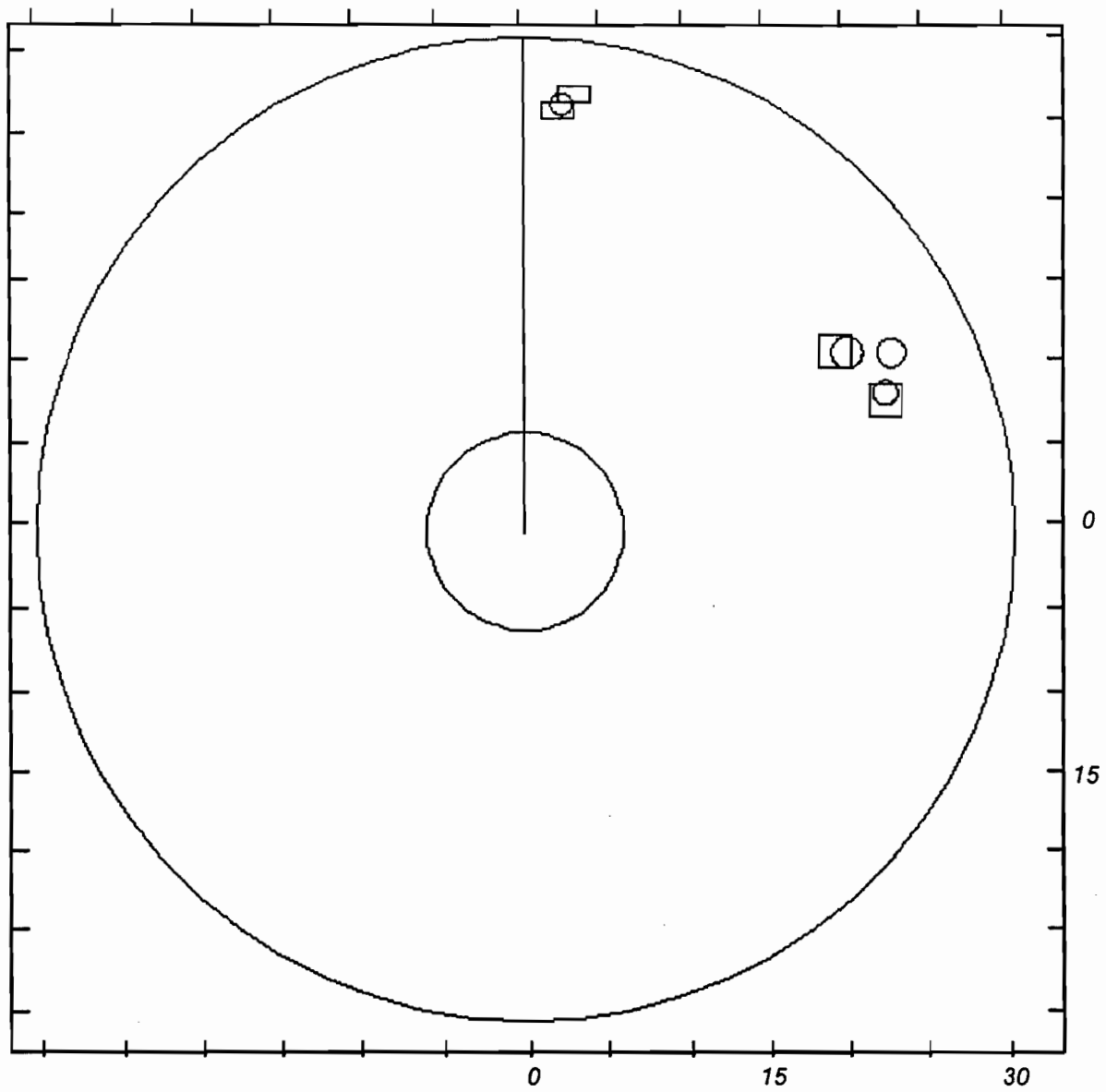

Figure 8. Algorithm/Truth Scoring Plot

ASP declares a hit where the region and truth overlap. Circles represent truth, rectangles are algorithm output. Tick marks are 5 km apart. Largest circle is at 30 km from radar, located at the center. This plot is of data from July 25, 1986, Huntsville, AL, at 22:01:01 GMT. The scan was at an elevation of 9 degrees, with a PRF of 900.

5.1.2 POD, PFD, and DTR

When all comparisons for the case have been made, various performance statistics are computed. The total number of truth hits divided by the total number of truth observations gives the probability of detection (POD) for the algorithm. The PFD, or probability of a false detection, is calculated as

1 – (total number of region hits) / total number of regions

The number of region hits is determined by taking the total number of regions generated, then subtracting the number of false, early, or late detections. In this calculation, therefore, early and late detections are not being considered as hits.

The detections–to–truth–ratio (DTR) is calculated by dividing the total number of detected regions by the total number of truths. This ratio gives a measure of the algorithm's "neatness," indicating the degree to which it is being discriminating in its issuance of detection. Ideally, it is desirable to have a DTR as close to unity as possible.

5.2 EVENT SCORING

5.2.1 Definitions

The scoring program also provides another aspect of evaluating algorithm performance, which is the computation of an *event recognition rate* (RR). By definition, an event is a group of truth observations occurring over time within the life span of a microburst. When truth is generated by the meteorologist, the rotation observation identified is associated with a named microburst event. A separate association post–algorithm–processing operation is performed on the algorithm output so that it can be scored on an event basis because the rotation algorithm itself does not group its regions into events.

The association program groups regions into events by evaluating temporal, spatial, directional, and altitude nearness criteria. Once the regions have been put into events, the RR is determined as follows. If at least one region hits a truth at any time during the truth event, that event is considered as having been recognized by the algorithm. If a detection occurs *early* with respect to the first observation of an event, then the event has been recognized *early*. Similarly, if a detection occurs *late* with respect to the last observation of the event, then the event has been recognized *late*. The RR is the number of recognized events divided by the total number of events.

Event scoring is interesting because the POD is usually much higher than with scoring on an observation–by–observation basis. It shows that the algorithm is able to detect some part of an event, and probably missed hitting some observations of the event along the way because of inconsistencies in the data. The existence of early and late recognition of the event may be significant with regard to microburst prediction capabilities, since the

more timely the detections for precursors such as rotation, the higher the confidence level of the initial outflow detection. [9] Late recognitions of events indicates over-sensitivity of the algorithm, causing it to continue to identify rotation regions even after the windfield has started to decay, implying the need for further parameter adjustment.

5.3 TRUTH GENERATION

5.3.1 Truthing Conditions

When scoring the performance of an algorithm it is important to take into consideration the conditions under which the truth was generated. As stated in section 3.2.1, the algorithm operates on pre-processed data in order to reduce the amount of data ambiguities. The meteorologist, however, works with raw data and performs visual interpolations over the incongruities of the data. This is especially significant with regard to signal-to-noise thresholding, and the ramifications of this will be discussed in Chapter 6.

When a rotation region is identified by the truther, the truth observation is expressed as a line segment spanning the two points that have the maximum velocity difference within a rotation region. For scoring purposes, the line segment is considered to be the diameter of a circle. This circle is used for the geographical comparisons with the algorithm regions. As a result, this circle may have an inaccurate area compared to the original rotation region identified by the expert.

In general, the meteorologist confines the search for rotation regions to the vicinity of microbursts and storms by identifying cells according to reflectivity characteristics. Conditions which give rise to other types of rotation are ignored by the truther. The rotation algorithm, on the other hand, has no knowledge of existing reflectivity regions and is therefore not as discriminating. More importantly though, the reflectivity information is used by the microburst recognition system *after* the feature extraction, so it is not clear that providing reflectivity data *during* feature extraction would improve overall performance of the microburst system.

The expert can also perform a time correlation with the data, looking forward and backward over the life span of the event in order to make decisions about the existence of rotation regions. This sort of time history association is not a part of the baseline microburst algorithm.

5.3.2 General Truth Characteristics

Figures 9, 10, and 11 are the results of a study to characterize rotation truth generated for Huntsville and Denver data. The histogram in Figure 9 shows that most of the line segments found by experts were about 1.5 km in length. Figure 10 shows that most of these segments have a velocity difference of about 13 m/s, and in Figure 11, the average shear value for the segment was about 9 $m/s \cdot km^{-1}$.

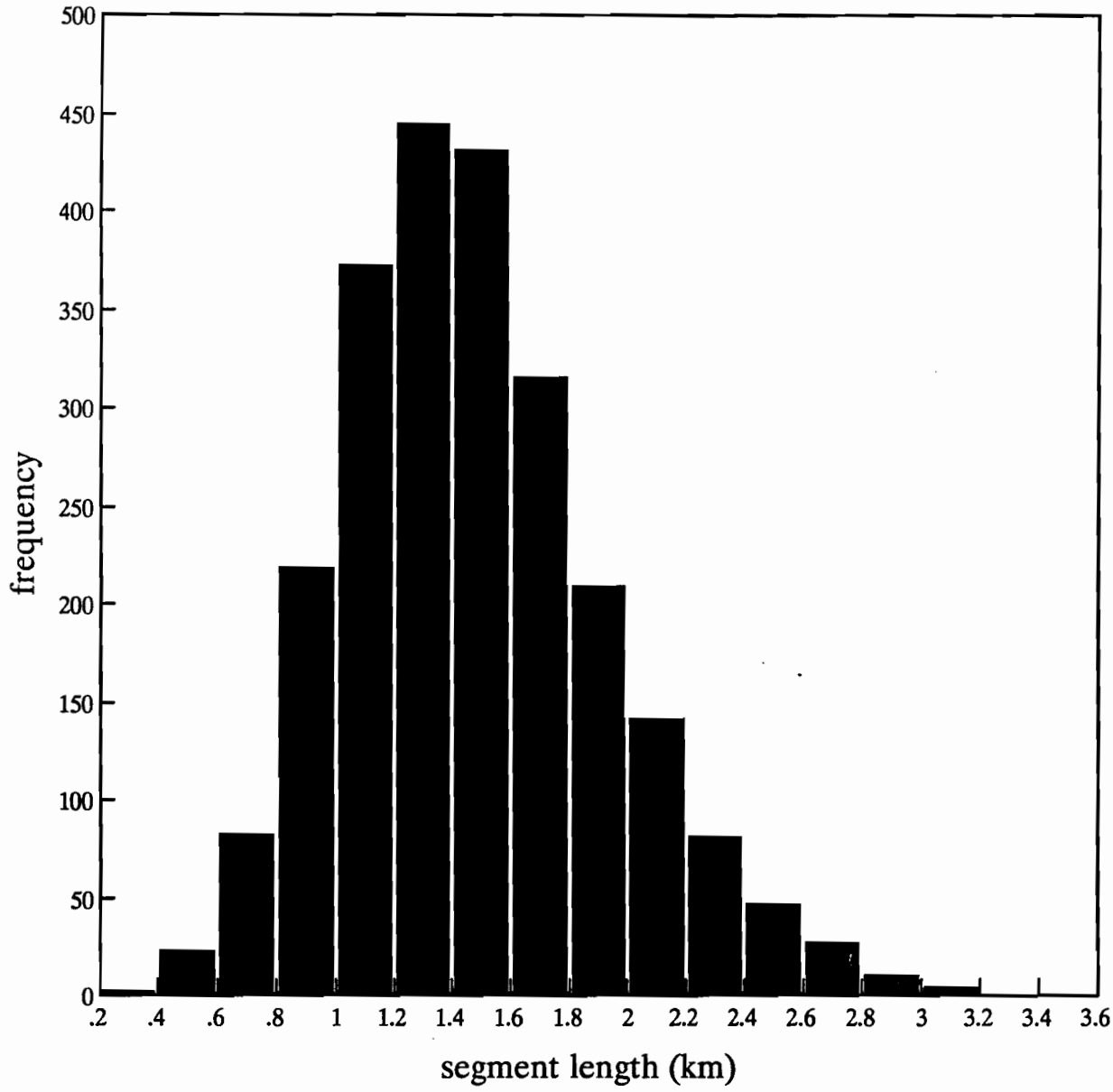

Figure 9. Rotation Truth Statistics: Segment Length

The histogram above shows that most of the rotation segments found by experts were about 1.5 km in length.

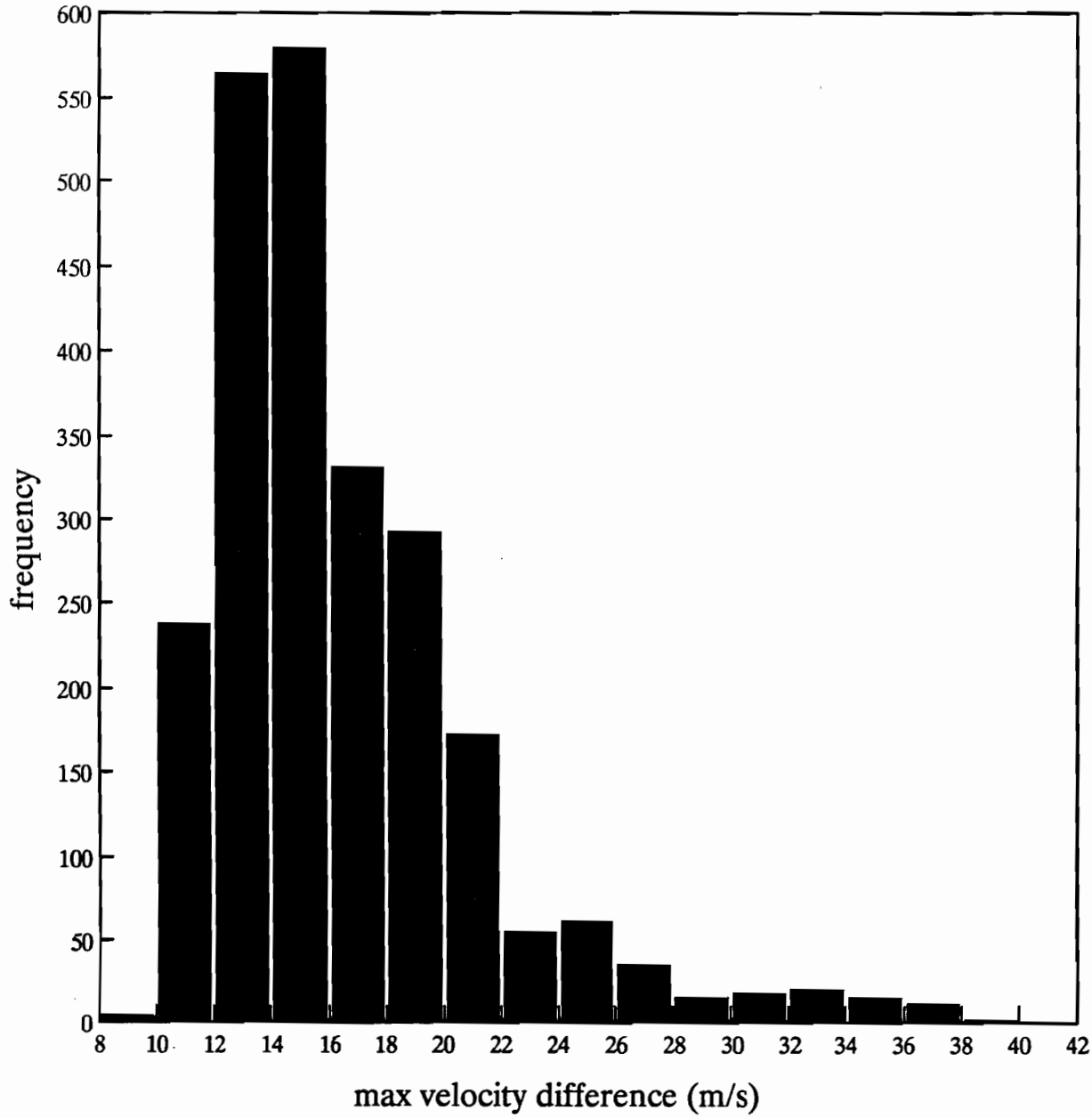

Figure 10. Rotation Truth Statistics: Velocity Difference

The figure show that most of the rotation segments found by experts have a velocity difference of about 13 m/s.

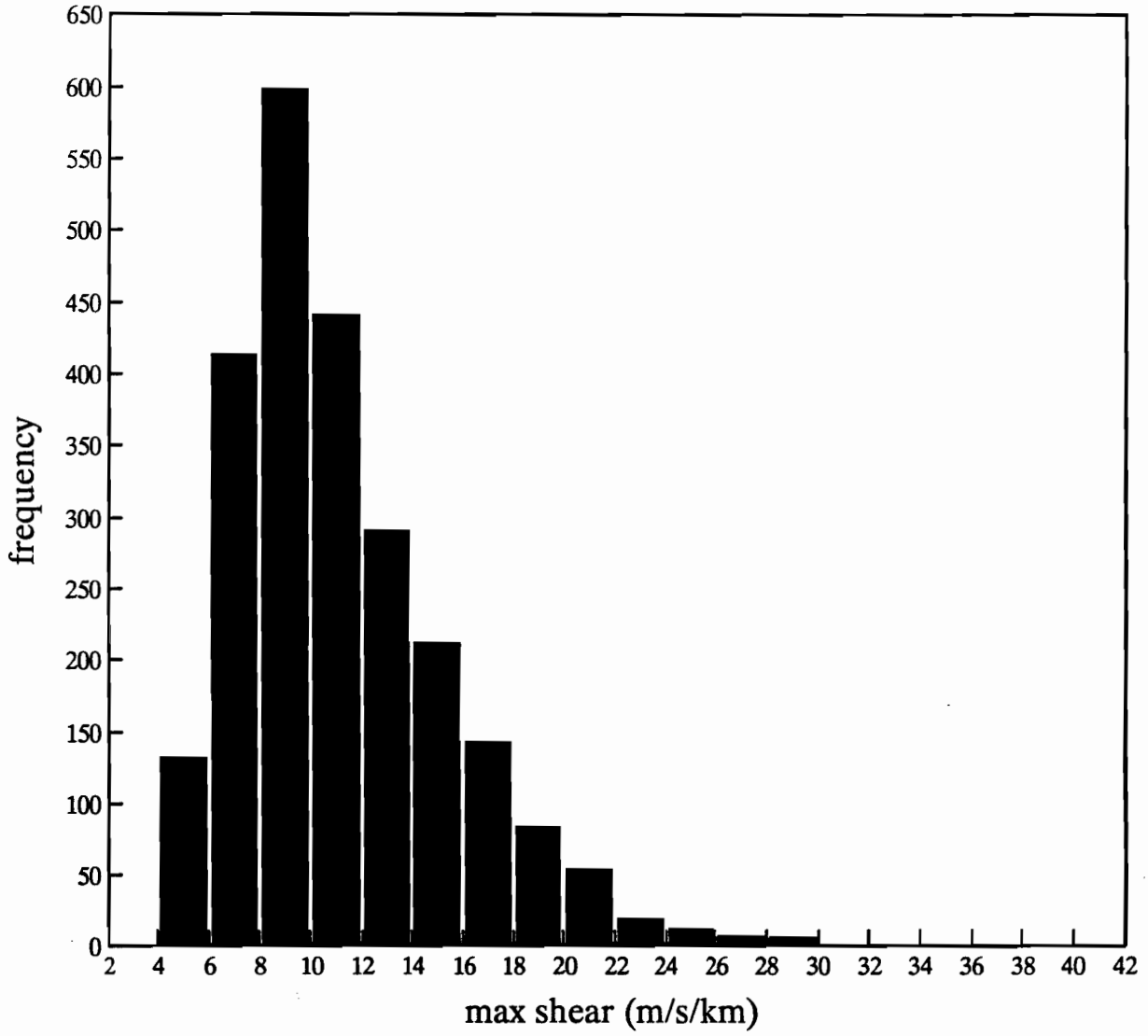

Figure 11. Rotation Truth Statistics: Shear

The figure shows that the maximum shear value for most of the rotation segments found by experts is about 9 $m/s \cdot km^{-1}$.

6. ANALYSIS OF RESULTS

6.1 SCORING RESULTS: TEST DATA

Table 3 shows the results of 13 test runs of the algorithm. Note that that **deltav_thr**, though listed as one of the parameters changed, is not included in the parameter list in Table 2 because its value was set to 10 m/s at the beginning of the testing and was never changed again. The values in the third column in Table 3 are a list of the parameters being varied for the particular test for each row in the table. For each test, the POD, PFD, and DTR were calculated and are also shown in the table.

The final test of the sequence yielded a parameter set which allowed for a POD of 100 percent for both Kansas City and Huntsville, with an average of 45 percent PFD.

One thing that can be seen from Table 3 is that as one test led to the next, the DTR first decreased for both Kansas City and Huntsville, reaching their low points on Test 6, then slightly increased, though with another local minimum at Test 12. This occurrence was mostly due to the manipulation of the **area_thr**, which eliminated a significant number of detections (both potential hits and false) when set to a value greater than 1.0 sq-km.

Perhaps the most noteworthy result is the complete failure of the tuning of these particular parameters in some cases to have any effect on the algorithm's performance for Denver data. The reason for this insensitivity turned out to be the extremely low signal-to-noise ratio (SNR) on the scans under test. At low signal-to-noise-ratio, there are many data gaps due to low SNR editing. As mentioned in section 5.3.1, the meteorologist accounted for this and still found a truth region, but the algorithm could not detect rotation regions with the large number of data gaps. Figure 12 shows a typical example where the use of SNR threshold eliminates a number of large anomalous velocities at the expense of assigning bad values to data in a valid rotation region.

Table 3.

Algorithm Improvement Results -- Test Data, by Site

test #	change #*	value	POD(%)	PFD(%)	DTR
		Kansas City			
1	2,1	10,0.0	70	73	8.5
2	1	0.4	70	81	7.8
3	1	0.6	70	76	7.2
4	1	0.8	90	84	5.7
5	3	500	80	81	4.4
6	4	2.0	60	60	2.0
7	4	1.5	70	69	2.9
8	5	-1.3	80	66	3.2
9	5,4	-1.3,2.0	70	60	2.5
10	5,4	-2.3,2.0	80	60	2.7
11	3	240	80	61	3.4
12	3,5,4	240,-2.3,1.5	70	57	2.3
13	4,6	1.0,0.5	100	61	3.8
		Denver			
1	2,1	10,0.0	0	0	0
2	1	0.4	0	0	0
3	1	0.6	0	0	0
4	1	0.8	0	0	0
5	3	500	0	0	0
6	4	2.0	0	0	0
7	4	1.5	0	0	0
8	5	-1.3	0	0	0
9	5,4	-1.3,2.0	0	0	0
10	5,4	-2.3,2.0	0	0	0
11	3	240	0	0	0
12	3,5,4	240,-2.3,1.5	0	0	0
13	4,6	1.0,0.5	0	0	0

Table 3. (cont.)

Algorithm Improvement Results -- Test Data, by Site

test #	change #*	value	POD(%)	PFD(%)	DTR
		Huntsville			
1	2,1	10,0.0	100	17	1.3
2	1	0.4	100	17	1.3
3	1	0.6	100	17	1.3
4	1	0.8	100	11	1.0
5	3	500	100	13	0.89
6	4	2.0	89	25	0.44
7	4	1.5	89	17	0.67
8	5	-1.3	89	17	0.67
9	5,4	-1.3,2.0	89	25	0.44
10	5,4	-2.3,2.0	89	25	0.4
11	3	240	100	10	1.1
12	3,5,4	240,-2.3,1.5	89	17	0.67
13	4,6	1.0,0.5	100	20	1.1

**The meaning of the change numbers in the second column are explained below:*

#	parameter changed
1	shear_drop
2	deltav_thr
3	range_thr
4	area_thr
5	az_thr
6	min_seg_len

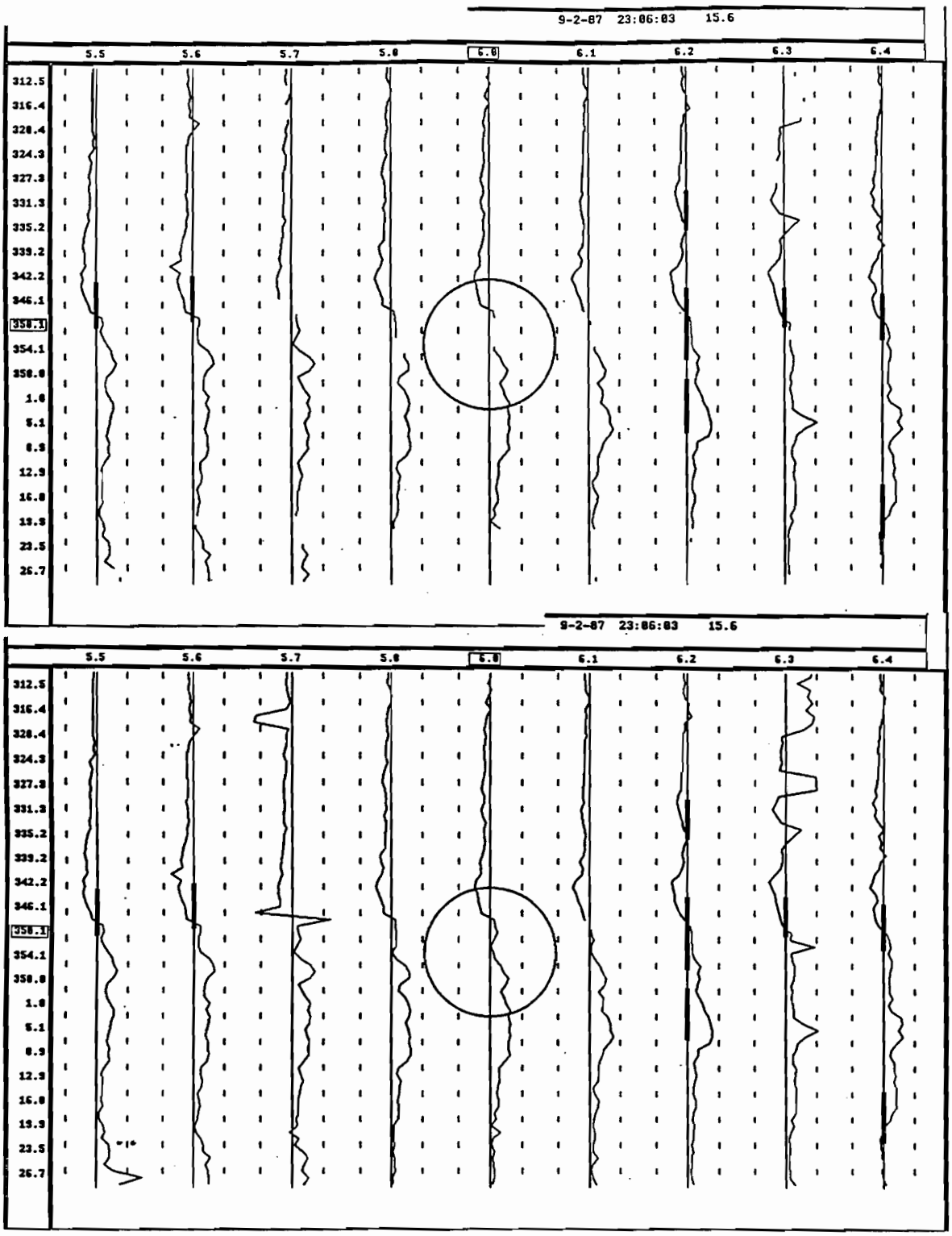

Figure 12. Azimuth vs. Velocity: Signature Analysis.

The plot is showing the azimuthal velocity signatures for a group of consecutive range gates. The top figure shows the effect on the data after SNR thresholding and velocity unfolding. The bottom figure shows data that has not been pre-processed. The circle is truth; the rectangles vertically overlapping the signatures are algorithm-generated shear segments. The dashed lines are +15 and -15 m/s about the velocity axis (solid vertical lines). The top is labelled in km, the left in degrees.

Kansas City data seemed to be most sensitive to the **shear_drop** threshold since the high environmental wind component typical of the geographical area caused many false segments to be identified. By allowing more flexibility in the requirements for growing a segment, the POD was improved for Kansas City, although its PFD then suffered. This effect is shown in the color radar plot in Figure 13, where the red rectangle is an algorithm bounding box overlaid on the radar data. This box is a false detection, where an intermediate version of the algorithm mistakenly detects the gradual change in wind velocity over the broad region of the scan as a genuine azimuthal shear.

One of the effects of using the final combination of all these thresholds is illustrated in Figure 14 in which the shear segments as well as algorithm bounding boxes are pictured. In this case, shorter segments led to a significant decrease in the PFD by giving rise to regions with insufficient area to be considered as valid output data.

Overall, the number of valid segments found was quite a bit higher with the final version of the algorithm. For Test 1, there were 4258 unused segments (segments whose associated region was invalidated by thresholding), and 709 belonging to 64 valid regions. For the final test, there were 7177 unused segments, with 824 belonging to 68 valid regions. This was to be expected because the goal was for a coarser, less sensitive, and thereby more effective detection capability, which is made possible by generating more numerous, though shorter, segments.

At least for higher reflectivity environments such as Kansas City and Huntsville, it can be said that the algorithm performance was improved in general by tightening the range association criterion from 1 km to 240 m and relaxing the requirement of a 1 degree in azimuth overlap to allowing a gap of 2.3 degrees. The fact that Denver's microbursts tended to have generally lower differential velocities, as well as less precipitation, [9] made detection more difficult there. In addition, reducing the segment length threshold, **min_seg_len**, made a dramatic difference in performance for Kansas City and Huntsville, improving the POD by as much as 30 percent, while increasing the PFD only a small amount. Shortening the segment length threshold from 1 km to 0.5 km works in conjunction with the association thresholds to allow short segments to be grouped together, thereby allowing the algorithm to be successful in a noisy velocity environment.

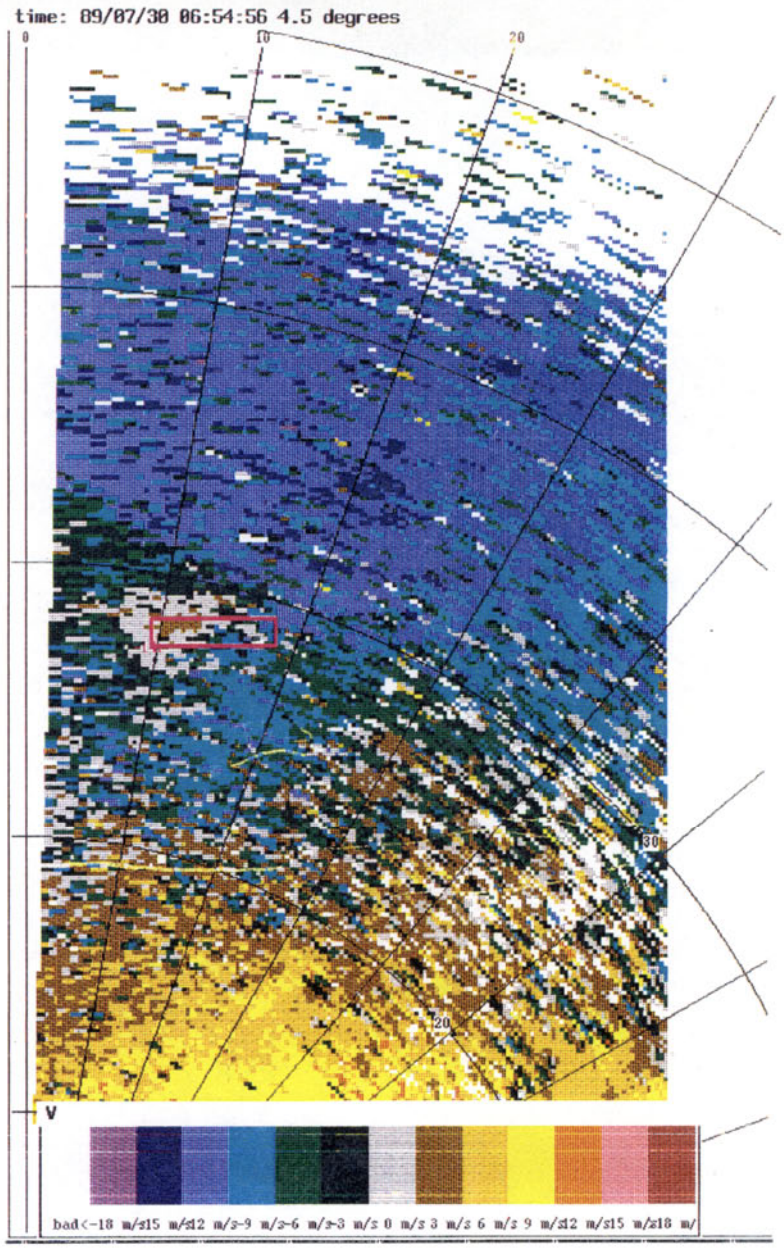

Figure 13. Resampled radar data with overlays: False detections.

A Terminal Doppler Weather Radar image from Kansas City, MO, on July 30, 1989, at 06:54:56 UT at an elevation angle of 4.5 degrees. The color bars at the bottom shows the velocity mapping in m/s. Azimuth lines are 5 degrees apart, range–rings are 5 km apart. Red rectangle is a false rotation detection.

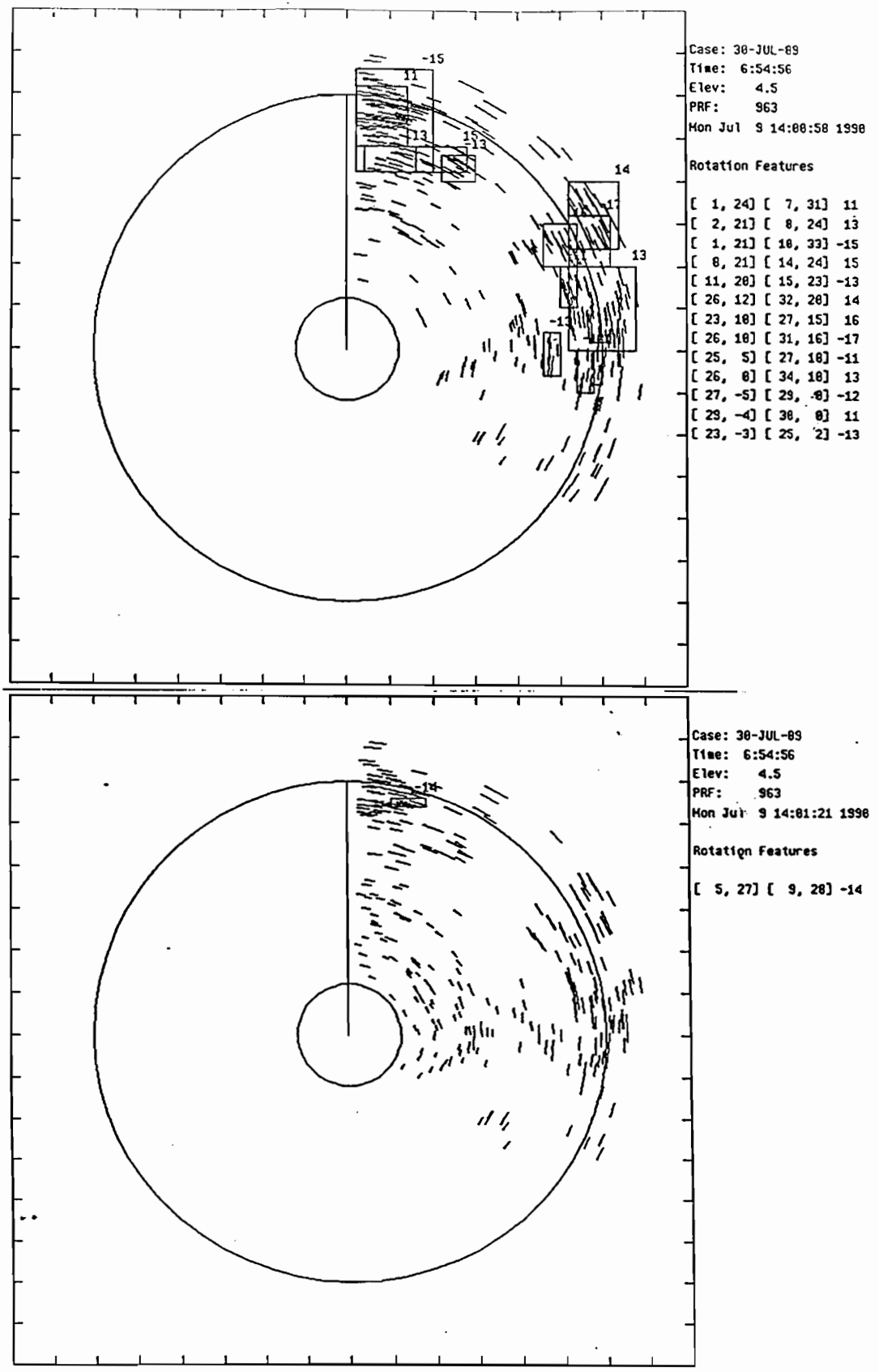

Figure 14. Comparison of results--First Parameter Set to Last Parameter Set

One of the effects of using the final combination of all these thresholds is illustrated above. Pictured here are the shear segments, as well as algorithm bounding boxes, which are all false detections. The top plot shows the output from the algorithm using the first parameter set; the bottom shows the output from the last parameter set. Note the shorter segments and reduction in number of regions in the bottom plot.

6.2 SCORING RESULTS--CASE DATA

Once it became apparent as to which logic and parameter changes to incorporate into a final version, called Version 1.5, the algorithm was run on the large data set. The complete set of results, arranged by case data and location, are given in Table 4. A quick overall comparison of Versions 1.4 and 1.5 is shown below.

	POD	PFD	DTR
wet	89	54	2.9
dry	59	60	1.9

Version 1.4

	POD	PFD	DTR
wet	84	37	2.1
dry	40	64	1.5

Version 1.5

wet = Kansas City and Huntsville
dry = Denver

It can be seen that the algorithm has an obvious sensitivity to the geographical region from which radar data is obtained, and so parameter tuning to improve algorithm performance must be done on a regional basis. This conclusion was also arrived at from the discriminant analysis, which will be seen in section 8.1. Therefore, it was most sensible to separate the final results into high reflectivity (wet) and low reflectivity (dry) region performance. High reflectivity is considered to be above 45 dbZ, and low reflectivity is 15 dbZ. The performance degradation seen for the low reflectivity results was because of the method of parameter tuning, and this will be discussed further in section 6.4.

While Version 1.4 was preferred for Huntsville and one case date (July 1, 189) in Kansas City, Version 1.5 was better for the other case date in Kansas City, July 30, 1989.

Overall, the results are that the variation of parameters can significantly decrease the DTR, which is desirable, and this will also decrease the PFD, but with a small decrease of the POD. At most, the POD was reduced by nine percent for Kansas City and Huntsville. However, roughly one-third of the detections were lost for the Denver case, with the result that the POD dropped by 19 percentage points.

The reduction in PFD was most significant for the Kansas City data, which could be made as low as 15 percent. This reduction in PFD was achieved with a reduction of only three percent in POD.

Table 4.

Final Scoring Results -- Case Data, by Site

Version	date	truth	hits	regions	region hits	POD	PFD	DTR
Kansas City								
1.4	jul01_89	428	354	652	461	83	30	1.5
using 1.0 km min. alt.,1.0 sq-km area								
1.5	jul01_89	414	333	530	448	80	15	1.3
using 0.5 km min. alt.,1.0 sq-km area								
1.5	jul01_89	414	338	563	450	82	20	1.4
using 1.0 km min. alt.,2.0 sq-km area								
1.5	jul01_89	414	333	548	448	80	18	1.3
1.4	jul30_89	304	292	1473	513	96	65	4.8
using 1.0 km min. alt.,1.0 sq-km area								
1.5	jul30_89	303	268	752	416	88	45	2.5
using 0.5 km min. alt.,1.0 sq-km area								
1.5	jul30_89	303	271	911	485	89	53	3.0
using 1.0 km min. alt.,2.0 sq-km area								
1.5	jul30_89	303	268	752	416	88	45	2.5
Denver								
1.4	sep02_87	140	82	272	107	59	60	1.9
using 1.0 km min. alt.,1.0 sq-km area								
1.5	sep02_87	134	48	129	64	36	50	0.96
using 0.5 km min. alt.,1.0 sq-km area								
1.5	sep02_87	134	54	206	132	40	64	1.5
using 1.0 km min. alt.,2.0 sq-km area								
1.5	sep02_87	134	48	129	64	36	50	0.96
Huntsville								
1.4	jul25_86	42	41	134	65	98	51	3.2
using 1.0 km min. alt.,1.0 sq-km area								
1.5	jul25_86	42	38	99	53	90	46	2.4
using 0.5 km min. alt.,1.0 sq-km area								
1.5	jul25_86	42	38	103	53	90	49	2.5
using 1.0 km min. alt.,2.0 sq-km area								
1.5	jul25_86	42	38	99	53	90	46	2.4

Three different types of scoring was performed on Version 1.5, as shown in Table 4. There are two thresholds in the rotation algorithm that are set to different values than the corresponding values in the microburst recognition system. These are the minimum altitude threshold and the minimum area threshold, which are set to 0.5 km and 1.0 sq-km, respectively, in the rotation algorithm and 1.0 km and 2.0 sq-km in the microburst recognition system. Since *ASP* has the ability to vary these parameters for scoring purposes, it was interesting to see the difference in performance statistics.

It may be noted that there are slight differences in the number of truth observations within the same case data when run on different versions. This is because of a scoring philosophy which states that truth must reside within the same 35 km limit as regions in order to be used for scoring. If not, it is eliminated from the scoring process and will not be counted in the total number of truth observations. If a region hits it, however, then it *is* included in the total, and the detections will be counted as hits. Therefore, if a particular run of the algorithm fails to produce a particular region, then it is possible that the truth observation corresponding to it will be ignored in the POD calculation if it is outside the 35 km radius of the scoring region.

6.3 EVENT SCORING RESULTS

Scoring the algorithm on an event basis resulted in an event recognition rate of 94 percent for higher reflectivity regions and 78 percent for low reflectivity regions. There was no change in the RR for Kansas City and Huntsville between Versions 1.4 and 1.5, but for Denver, the RR dropped by 11 percentage points. The event scoring is given in Table 5, showing also the number of events having early or late detections. One would expect these results to be analogous to the observation scoring in the previous section.

Table 5. Event Scoring Results

Version	date	truth	hits	regions	region hits	POD	PFD	DTR
				Kansas City				
1.4	jul01_89		8		7	7	7	88
1.5	jul01_89		8		7	7	7	88
1.4	jul30_89		6		6	6	6	100
1.5	jul30_89		6		6	5	5	100
				Denver				
1.4	sep02_87		9		8	6	8	89
1.5	sep02_87		9		7	4	4	78
				Huntsville				
1.4	jul25_86		3		3	3	3	100
1.5	jul25_86		3		3	3	3	100

6.4 DISCUSSION

The first issue to be addressed is the apparent discrepancy in performance between the results for test data and for case data. Some difference was expected, however, given the difficulty of choosing a generic set of test scans. In addition, the test data was biased toward producing false rotation regions since the major goal in improving the algorithm was to reduce the PFD. Before the testing commenced, however, it was not known that the Denver data would essentially drop out of the evaluation, with its especially difficult representative scans. It was also discovered later how sensitive the parameter tuning was to the region associated with a data set. Therefore, the ultimate parameter settings were effectively geared toward performance under conditions of high reflectivity.

It is clear, however, that although the POD was greatly improved for the twenty-scan-test-data set, it was made somewhat worse for the case data set of 588 scans. This was because of the overall tendency of the final parameter set to allow for shorter segments. Since the area of a region is calculated by totaling the areas of all its constituent segments, the important effect of having shorter segments was to reduce the overall area for a candidate region. This means that the test data scans, which happened to cause the algorithm to detect a large numbers of segments, would now declare as valid a region it had previously discarded because it was too large. Therefore, what would have been a miss was now a hit. These regions apparently had areas well in excess of the area criteria. For the case data, the characteristic of shorter segments statistically had more of an effect on reducing the number of regions generated. The average area for rotation regions identified by Version 1.4 is 3.57 sq-km, whereas for Version 1.5 it is 2.5 sq-km, a decrease of 32 percent. Therefore, if a region detected by Version 1.4 was small enough to begin with, a reduction in its area by an average of 32 percent would lead to its invalidation by Version 1.5, and thus the POD was reduced.

A number of general observations can be made here with respect to the scoring results. One is that the misses were generally caused by the absence of a rotation region declaration, as opposed to the declaration of region that was too distant from a truth region. That is, there were no spatial near-misses. If the algorithm missed a detection, it was because of one of two reasons. First, if too few segments were generated for the region, usually due to low signal-to-noise ratio, the area of the resulting region would be too low to be considered valid, as with Denver data. Second, if too many segments were generated, as with strong environmental winds, the region would be eliminated for having too large an area.

A strong environmental wind could introduce false detections because the algorithm detects only monotonically increasing (or decreasing) velocities, not necessarily passing through zero from negative to positive. Inhomogeneities in the windfield would cause the algorithm to interpret changes in the wind speed as the endpoints of shear segments. In Figure 15, the area within the circle represents part of a radar scan, centered on the radar. A horizontal eastward wind is shown as dotted lines. The length of the solid arrows represent

the magnitude of the the radial components of a the wind as seen by the radar. The darker arrows indicate radial velocities away from the radar, and the lighter arrows are velocities toward the radar. At due north and south, the radial component of the wind is zero, while at east and west the radial component of the environmental wind is a maximum. If the area of the horizontal wind were within the size parameter of the algorithm and were of sufficient intensity, this would result in the false detection of a rotation region. The box represents such a false detection.

A second related point is how relatively infrequently detections were early or late rather than false. This is illustrated in Figure 16, where the number of each type of detection is plotted opposite the cases label. The points in this diagram were sorted in ascending order of the number of false detections to produce a graph that would clearly show the relationships. One interesting observation is that when the total number of regions was relatively small, there were roughly as many early and late detections as false detections. When the total number was large, however, there were many more false detections than early or late detections. The reason for this is similar to the observation above regarding misses, since early and late detections have a close spatial relationship to some truth observation, being displaced from it only in time. This happens when there are slightly different data conditions on successive scans, making it possible for the overlap to occur with truth on a scan before or after the algorithm's declaration, though it misses the current scan. The case of a detection being declared early or late, for the reasons given in the preceding paragraph, should therefore occur infrequently with respect to the total number of detections. By noting the different scales on the y–axes of the figure, one can also see the difference in overall region production in Version 1.4 as compared to Version 1.5.

Because the design of the current TDWR testbed real time feature extraction system is to process one radial at a time, it was not possible for the rotation algorithm to have an entire scan's reflectivity information, so it could not make any association with storm cells identified in the reflectivity image. The microburst algorithm, on the other hand, can discard rotation regions that are not spatially near a reflectivity structure, but the result is that the rotation algorithm appears to have a high PFD.

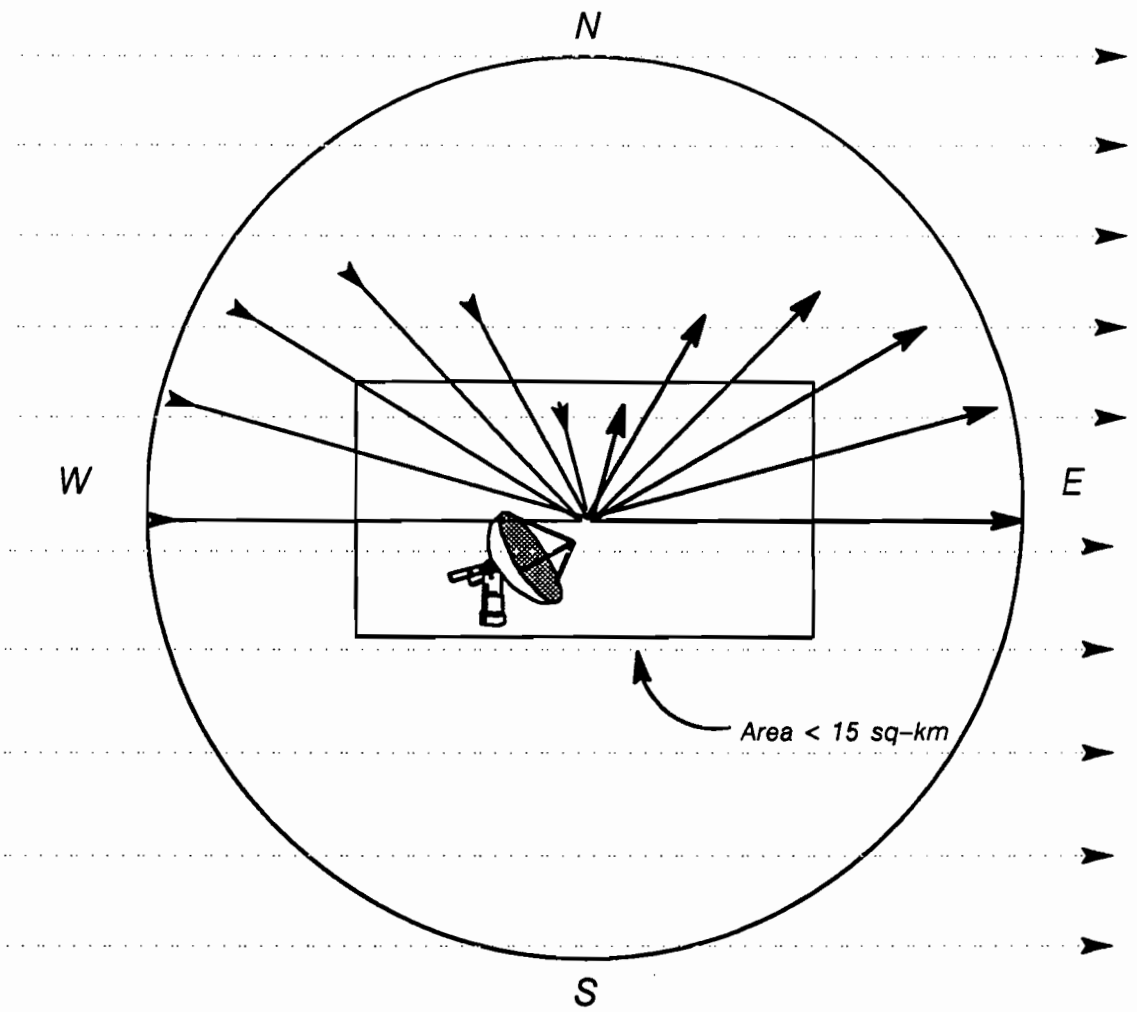

Figure 15. How an Environmental Wind Can Cause False Detections.

The area within the circle represents part of a radar scan, centered on the radar. A horizontal eastward wind is shown as dotted lines. The length of the solid arrows represent the magnitude of the the radial components of the wind as seen by the radar. The darker arrows indicate radial velocities away from the radar, and the lighter arrows are velocities toward the radar. At due north and south, the radial component of the wind is zero, while at east and west the radial component of the environmental wind is a maximum. If the area of the horizontal wind were within the size parameter of the algorithm and were of sufficient intensity, this would result in the false detection of a rotation region. The box represents such a false detection.

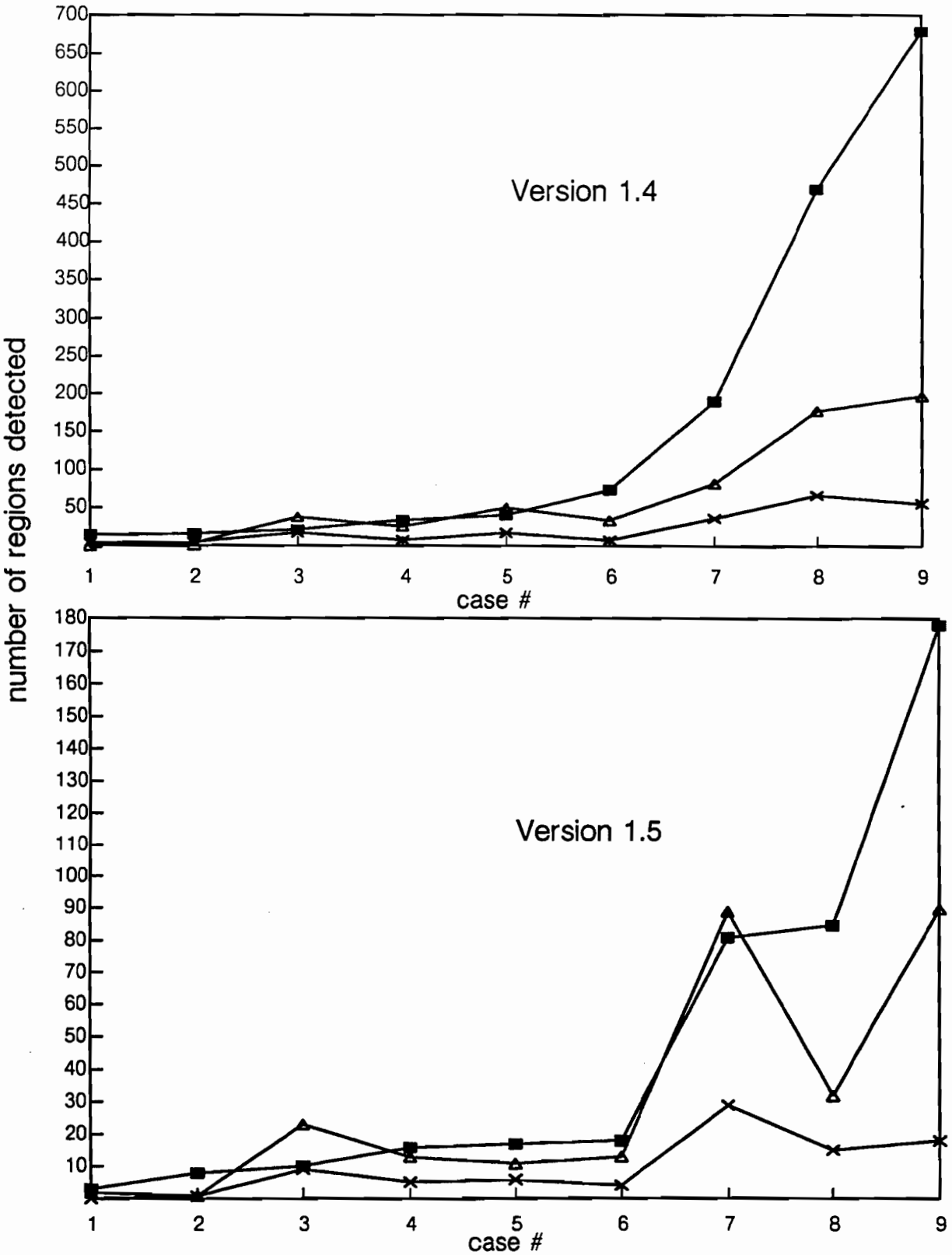

Figure 16. Relative Distribution of Detections.

Detections were more likely to be classified as false than as early or late for the nine different cases plotted. The point symbols are: ■ false, Δ early, × late.

In retrospect, if an entire scan's worth of data were to be stored, then two-dimensional image processing techniques could be performed. The advantage is that the two-dimensional techniques are more well known that the one-dimensional approach being taken here. Furthermore, using such a technique would produce a set of rotation regions that could be retained for correlation with regions found in subsequent scans, resulting in a measure of the persistence of a detection. Even with the data buffered, given the current scan strategy stated in section 2.1.3, time correlation would be restricted to a 2.5 minute sampling of a particular altitude, which is less than satisfactory for a short term event such a microburst.

Given that further validation and rejection of rotation regions is done at the microburst algorithm level, which is subsequent to the feature extraction phase (see section 2.1.2), there is no good criteria at this time for acceptable POD and PFD for rotation detection.

Lastly, on the whole, the process of improving the rotation algorithm provided valuable insights into its weaknesses, strengths, and sensitivities on a per-locale basis. The algorithm can be successful only if its parameters have been tuned to the environment in which it will be used. The algorithm performed best in high reflectivity environments because this provided a high SNR, and therefore a smoother signature, such as those shown in Figure 17. Furthermore, it was found to be impossible, in practice, to raise the POD without also raising the PFD, given the amount of information the algorithm has at its disposal.

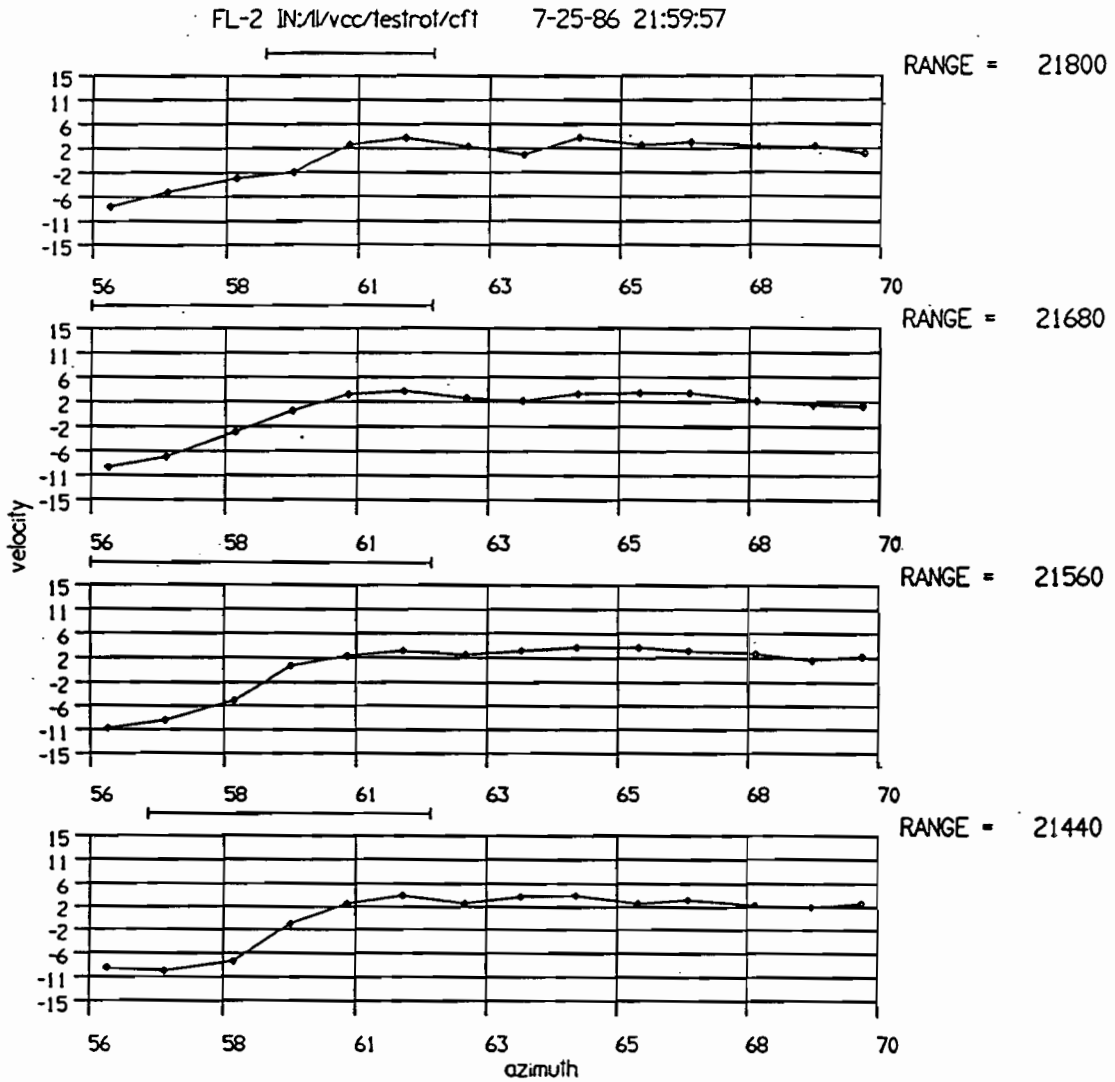

Figure 17. Sample Rotation Signatures: Huntsville, AL.

Plots of velocity as a function of azimuth for four consecutive range values for test data from Huntsville, AL on July 25, 1986, at 21:59:57 UT. Scan direction is counter-clockwise, which accounts for the ranges in reverse order vertically. Long horizontal H-shaped bars represent algorithm shear segments, which delineate the sloping velocity signatures. The azimuth values are in degrees, the velocity axis is meters/second, and the range values are in meters.

7. SIMULATION STUDIES

7.1 INTRODUCTION

An alternative approach to analyzing the performance of the rotation algorithm is to simplify its data input, which would therefore alleviate the task of finding representative test data. This has been accomplished by utilizing a program that can generate simulated rotation regions. The additional advantages to this are obvious--the elimination of data contaminants such as clutter, velocity folding, and some inherent ambiguities of the scoring process, as well as achieving greater clarity (by definition) of the truth. All of this contributes to a higher confidence factor for the conclusions found.

The previous notwithstanding, the main reason to use a simulated data set is to verify the degree to which the algorithm "perfectly" detects a "perfect" rotation region. Perfection in this case is defined as a POD of 100 percent and a PFD of 0.

Six different data sets were created for use with three experimental versions of the algorithm, each with two different parameter sets. This chapter contains an analysis of these tests and offers some solutions.

7.2 PARAMETER DIFFERENCES

The parameter sets, called in this chapter **site** and **final**, differed as shown in Table 6. Any other parameters involved were the same in both parameter sets. The nature of the parameters listed in the table are explained in Section 4.4.2.

7.3 ALGORITHM VERSION DIFFERENCES

The three versions of the algorithm used for this study will be referred to here as **A**, **B**, and **C** for simplicity. The differences between them are briefly outlined below:

- **A** is the current operational version running at the testbed and is implemented as specified in the AEL. It shares a feature with Version B, described below, in that it will continue a segment even if velocities are constant.
- **B** has the shear validation test described in section 4.4.1, a type of segment cropping technique which allows a shear segment to grow only if its current shear value (equal to the segment's differential velocity divided by its length) will not decrease with the addition of the new azimuth gate. This is used to prevent a segment from becoming too long, even though the velocity difference between its endpoints may be of sufficient magnitude to pass a velocity validation test. The main difference between B and C is that B will continue to build a segment even if the velocities are changing only slightly.
- **C** has the three-radial buffering as described in Section 4.4.1, intended to accomplish some data smoothing. This procedure has the effect of smoothing the data

by "blurring" the data points. In addition, this version will end any segment it may have started if the difference between neighboring velocities is small enough (i.e., an absolute value less than or equal to **vel_thr**, which is currently set to 0).

7.4 TEST SUITE

The data for this study was produced by a program that synthesized radar image data according to a set of variable input parameters. The image contained a set of azimuthally sheared velocity points which form "perfect" rotation regions, such that its velocity vs. azimuth profile would appear as in Figure 4b. All of the simulated regions were elliptical, and centered at range and azimuth of 10 km, 45 degrees, measured with respect to the radar. The sheared region was oriented at 135 degrees from north, meaning that the velocity shear was aligned at 135 degrees. Those regions whose eccentricity was 1 as listed in Table 6 were symmetrical; the major axis = minor axis = 2 km. For those regions whose eccentricity was listed as 0.5, the major axis, parallel to the azimuth axis, was set to 2 km, and the the minor axis, parallel to the range axis, was 1 km.

For all of the simulated regions, the velocity in the area surrounding the sheared region was initialized to 0 m/s. An example of a simulated rotation region is shown in Figure 18 and the region attributes are summarized in Table 7.

Table 6.

Differences in the Parameter Sets

Parameter	SITE	FINAL
range_thr	1000 m	240 m
az_thr	0 degrees	-2.3 degrees
min_seg_len	1.0 km	0.5 km
deltav	7 m/s	10 m/s

Table 7.

Characteristics of the Simulated Data Test Suite

Case #	Velocity Differential (m/s)	Eccentricity
I	30	1
II	30	0.5
III	20	1
iV	20	0.5
V	12	1
VI	12	0.5

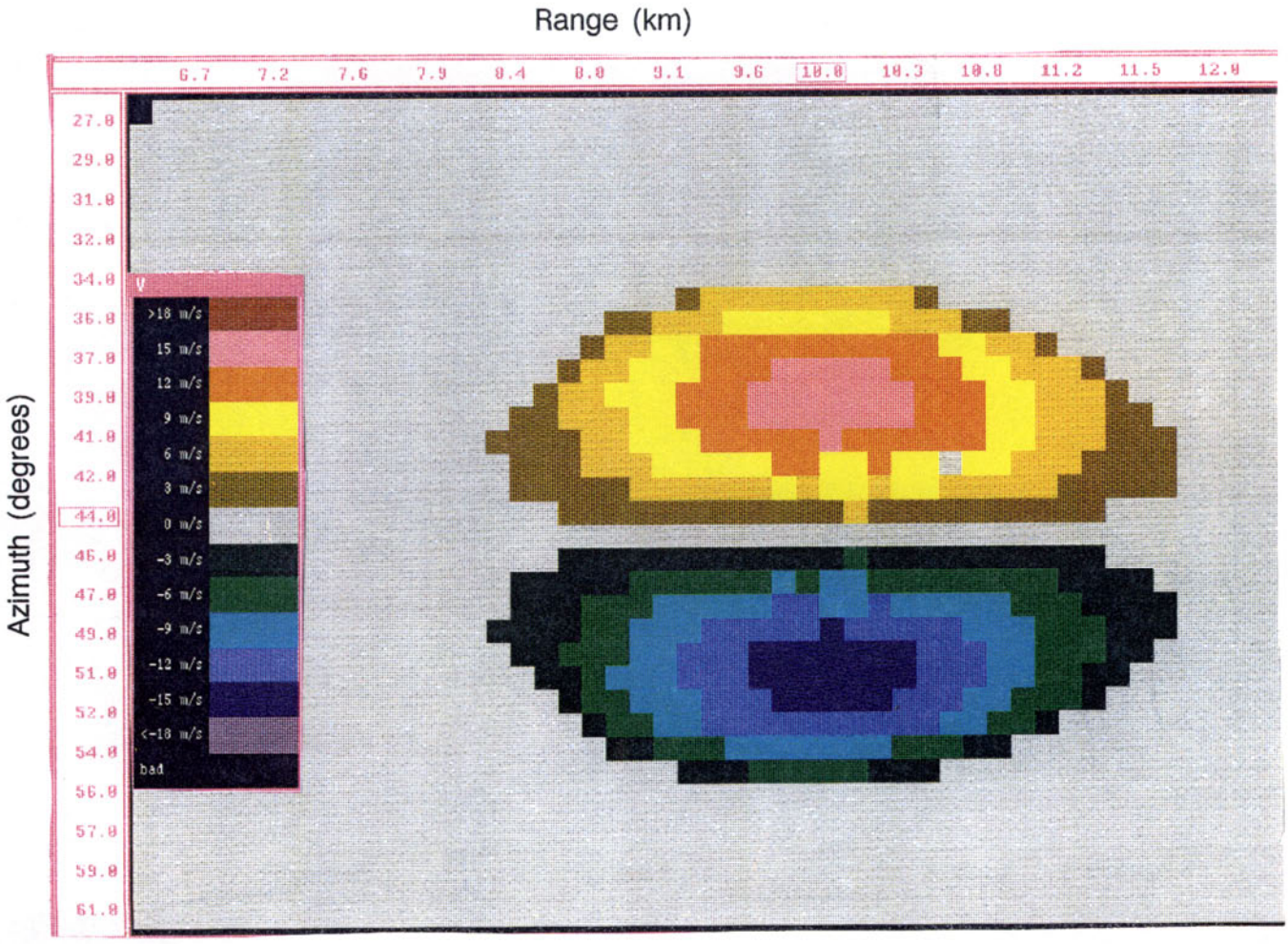

Figure 18. Polar Coordinate Plot of Simulated Rotation Region

Warm colors (red, orange) are representative of velocities receding from the radar, and cool colors (blue, green) represent approaching velocities. Top axis is range, labelled in km, left axis is azimuth in degrees.

7.5 TEST RESULTS

Because of the accuracy of truth in the case of simulated data, it was possible to evaluate the performance of the three algorithms on a different level than with real data. The scoring was performed on a point-by-point basis, where *each velocity point* identified by an algorithm as belonging to a valid segment was judged as either inside the truth region (valid), or outside the region (false). This gave a much finer resolution for the calculation of the POD and the PFD. The number of algorithm points inside the simulated region boundary divided by the number of truth points in this region gave the POD. The number of algorithm points outside the truth region divided by the total number of points generated by the algorithm gave the PFD.

Table 8 summarizes the performance of the three algorithms with the simulated data. Figure 19 shows a sample listing of the segments found by algorithm **A** using the **final** parameters for region VI.

Table 8.

Simulation Test Results: POD and PFD by Case

Version/parameter set						
CASE ▼	**A/site**	**A/final**	**B/site**	**B/final**	**C/site**	**C/final**
	POD					
I	100	100	97	97	98	98
II	98	100	90	90	89	89
III	100	100	98	98	100	100
IV	100	100	100	100	99	100
V	100	100	99	99	99	99
VI	100	100	99	99	100	100
	PFD					
I	15	36	12	25	13	14
II	11	23	6	9	7	8
III	20	38	18	22	17	19
IV	22	32	11	11	10	12
V	32	42	27	27	29	29
VI	31	41	25	25	24	24

STRTAZ	STPAZ	DV	SHR	RNG	MINV	MAXV
40.0	50.0	-6.6	4.1	9120	3.3	-3.3
40.0	50.0	-8.4	5.2	9240	4.2	-4.2
40.0	50.0	-9.2	5.7	9360	4.6	-4.6
40.0	50.0	-10.4	6.3	9480	5.2	-5.2
40.0	50.0	-11.6	6.5	10200	5.8	-5.8
40.0	50.0	-10.6	5.8	10440	5.3	-5.3
43.0	50.0	-7.9	6.1	10560	3.1	-4.8
40.0	50.0	-8.9	4.8	10680	4.4	-4.5
40.0	50.0	-7.4	3.9	10800	3.7	-3.7
40.0	50.0	-5.5	2.9	10920	2.7	-2.8
39.0	51.0	-11.2	5.6	9600	5.6	-5.6
40.0	51.0	-11.6	6.2	9720	5.8	-5.8
39.0	51.0	-11.8	5.7	9840	5.9	-5.9
39.0	51.0	-11.9	5.7	9960	5.9	-6.0
39.0	51.0	-11.8	5.6	10080	5.9	-5.9
39.0	51.0	-11.2	5.2	10320	5.6	-5.6

Figure 19. Sample Listing of Segments Found for a Simulated Region.

In the listing, STRTAZ is the starting azimuth of the segment in degrees, STPAZ is the ending azimuth, DV is the velocity differential in m/s, SHR is the shear in m/s/km, RNG is the range of the segment from the radar in meters, MINV is the minimum velocity endpoint of the segment in m/s, and MAXV is the maximum velocity endpoint.

According to Table 8, the best detection performance overall was that of version **A**, though its false detection rate was somewhat higher using the **final** parameter set. None of the algorithms performed absolutely perfectly, which would mean every single point in its proper place, but the POD never went below 89 percent, and rarely below 98 percent. The PFD was generally lower for versions **B** and **C**.

All of the algorithms generated the most false detections for the weaker regions (V and VI). The algorithms had the best detection performance for the moderate regions (III and IV). The lowest PFD's in general were for the strongest regions (I and II).

In all cases, the **final** parameters generated more detections than the **site** parameters, which resulted often in an increased POD as well as a higher rate of false detections.

Varying the eccentricity of the simulated region in cases II and IV appeared to have somewhat lowered the number of false detections in general. For algorithm **B** and case II, the asymmetrical region in combination with the higher shear caused the POD to drop 10 percent, and since the PFD was also lowered, the algorithm was producing fewer detections in general. Algorithm **B**'s behavior for case IV, however, is quite different, and so

there is no clear correlation here. In fact, since both regions caused B to detect the same number of segments, the difference is only in the length of the segments. In any case, more study is needed to determine the effect of asymmetry on detection of rotation.

The performance of the algorithms was also evaluated on the basis of the number of valid segments (belonging to an output region) found by the algorithms as compared with the number of truth segments in the simulated regions, and the results are given in Table 9. It can be seen from Table 9 that it is not sufficient to evaluate performance on the basis of the number of valid segments, since in every case the POD would be 100 percent.

In general, version **B** produced fewer segments than the other algorithms. In general the algorithms produced more segments than in the truth regions, and these were always along the edges of the region, where it is a judgment call by the truther what are the "true" boundaries of the region.

Table 9.

Number of Valid Segments for Algorithms and Truth by Case

case	A/site	A/final	B/site	B/final	C/site	C/final	Truth
I	27	28	27	28	27	28	25
II	20	20	17	17	17	18	19
III	25	26	25	26	25	26	23
IV	18	18	17	17	17	18	17
V	21	21	20	20	21	21	17
VI	16	16	16	16	16	16	14
total	127	129	122	124	123	127	115

7.6 CONCLUSIONS

7.6.1 For the Study

The algorithms in general performed better on the the stronger rotation regions, especially with respect to the frequency of false detections. Although the results of this study are not dramatic, they do show that the algorithms can detect a perfect rotation, but the region is over-detected.

The best performance on perfect data was that of version **A**, using the **site** parameter set. This is encouraging, because it verifies the correctness of the original design.

7.6.2 In General

The simulation study provided information that was actually more useful for decreasing the PFD (than for increasing the POD) by making it possible to isolate the sources of algorithm sensitivities that were not obvious from field data analysis.

The simulation was helpful also because it revealed the importance of the minimum segment length threshold. Earlier in the study, the tests were conducted in such a way that a particular parameter setting was preventing the algorithm from ever detecting the rotation region. The parameter was modified, and the tests were run again on regions large enough to be detected properly.

8. FUTURE WORK

8.1 DISCRIMINANT ANALYSIS

Since it would be beyond the scope of this report to provide a tutorial on discriminant analysis, it suffices to say that such an analysis is one that involves the problem of the classification of observations based on a set of measured **features** [10]. As it applies to improving the rotation algorithm, this would be the task of classifying detections as either "valid" or "false." This involves the specification of a distribution model through estimation of the mean feature vector and covariance matrix for each class. The covariance matrix shows the relationships and dependencies between the various features of a rotation region and their relative importance in classifying the detection. If this discriminant function were to be implemented in the rotation algorithm, then when a region had passed all its current validation thresholds, the probability of its being a valid detection would be calculated from the discrimination function metric. This, as a final test, would invalidate those regions it judged to be ultimately false detections and keep only those it considered valid.

In order to use the discriminant function, training data was required, and this consisted of algorithm output (Version 1.5) for the three sites, with each rotation region declaration being marked as valid or false by a comparison with truth. This formed the basis for the model, and the results of calculating the feature means and standard deviations are shown in Table 10. The features chosen were the region's velocity differential, the number of segments in the region, its area, maximum shear and average shear. The column labelled T^2 is a measure of how significant the feature is in its ability to distinguish the class of a detection.

8.1.1 Results

From the entries in the T^2 column it can be seen that the number of segments is the most important feature in determining whether an detection is valid, and in agreement with the parameter tuning research. This is borne out by the fact that the more successful versions of the algorithm were found to be the ones that declared more segments on the whole. Figure 20 shows the distribution of valid regions by the number of segments in them. Compare this to Figure 21, which shows the same for false detections, and the discriminating ability of this feature will become further apparent.

If this approach is to be used as an improvement to the algorithm, it will be best to train it on the data from the geographical area where the system will be running in order to obtain the most appropriate set of parameters. To obtain an upper bound on the performance improvements that can be expected, it was possible to get classification information for the case data using the case data itself as a training model. From the resulting statistics given in Table 11, it can be inferred, for example, that for Denver the number of false detections could decrease by 21 percent, at an expense of only 1 percent of its POD.

Table 10.

Discriminant Analysis Calculations

	False detections			Valid detections			
Kansas City							
Feature	*mean*	*stdev*	*count**	*mean*	*stdev*	*count*	*T2*
vel diff	12.97	3.33	1092	12.94	2.28	439	0.140
num segs	18.26	12.66	1092	28.09	14.26	439	13.232
area	4.22	3.24	1092	6.43	3.50	439	11.773
max shear	7.15	3.02	1092	7.13	2.58	439	0.079
avg shear	6.59	2.22	1092	6.72	1.68	439	1.047
Denver							
Feature	*mean*	*stdev*	*count*	*mean*	*stdev*	*count*	*T2*
vel diff	13.24	3.91	927	14.06	2.62	108	2.130
num segs	16.22	12.38	927	22.00	12.80	108	4.575
area	4.64	3.28	927	5.81	3.85	108	3.419
max shear	5.96	2.97	927	6.61	2.40	108	2.164
avg shear	5.84	2.29	927	6.36	1.80	108	2.256
Huntsville							
Feature	*mean*	*stdev*	*count*	*mean*	*stdev*	*count*	*T2*
vel diff	13.38	3.30	488	14.31	3.38	49	1.868
num segs	9.43	8.28	488	24.92	12.46	49	11.800
area	3.10	2.39	488	5.96	3.23	49	7.682
max shear	7.46	2.99	488	8.41	3.62	49	2.070
avg shear	6.86	2.29	488	7.37	1.97	49	1.497

* *The* count *is the number of objects in each class used to calculate its mean.*

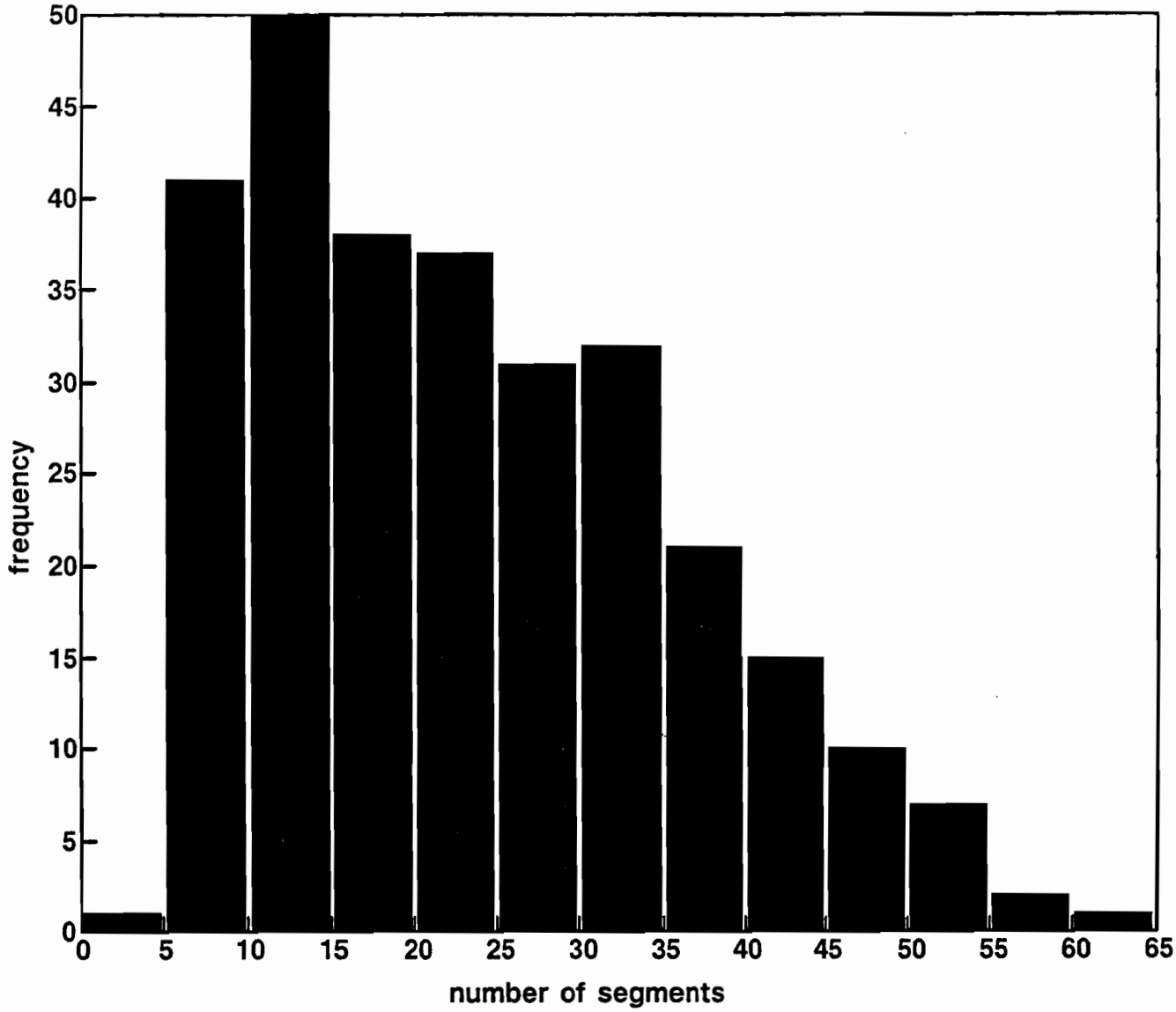

Figure 20. Number of Segments Distribution: VALID Detections

The figure shows the distribution of the number of segments for valid rotation region declarations.

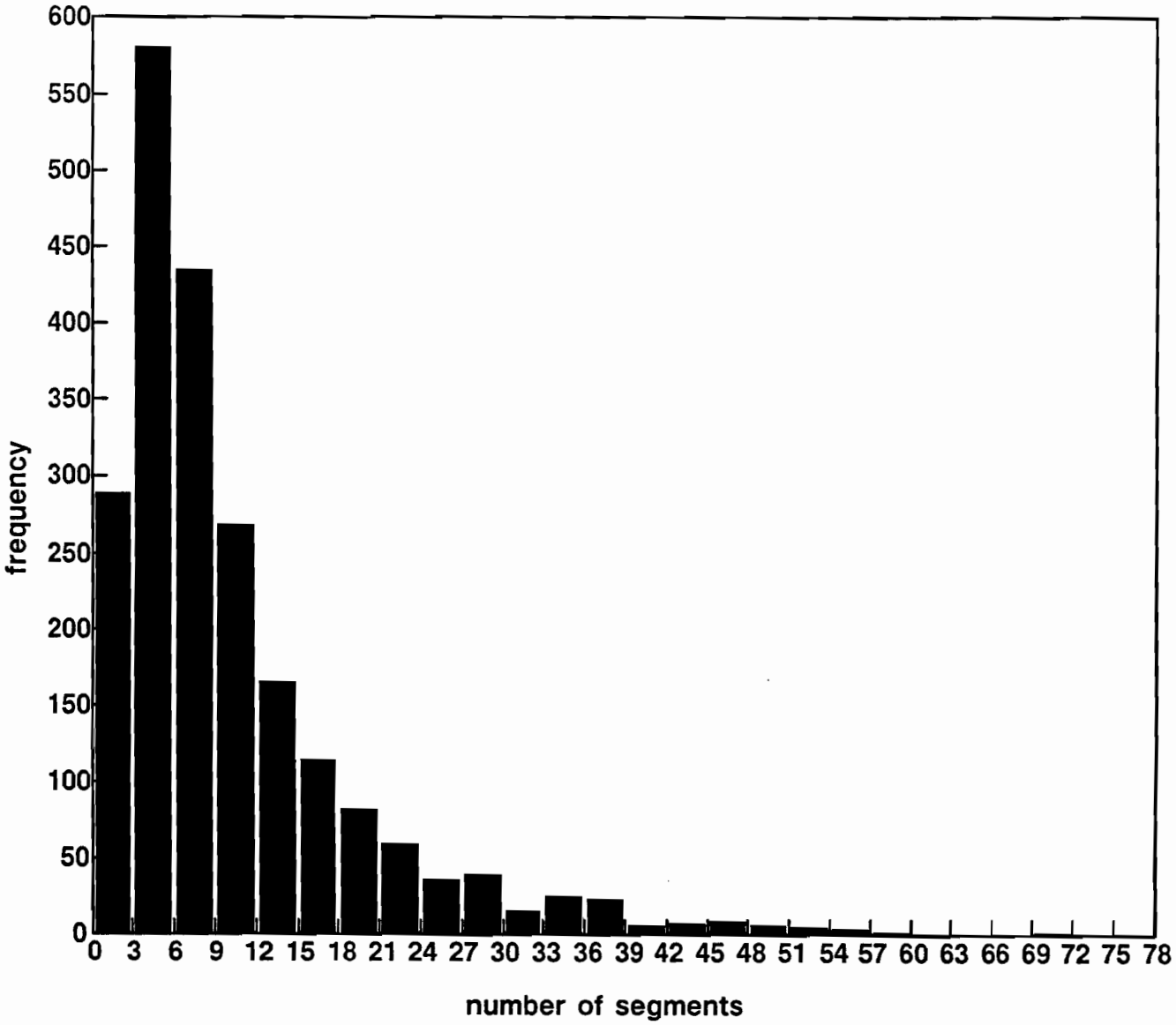

Figure 21. Number of Segments Distribution: FALSE detections

The figure shows the distribution of the number of segments for false rotation region declarations.

Table 11.

Results of Discriminant Analysis

Site	*valid regions kept*	*valid regions discarded*	*false regions kept*	*false regions discarded*
Kansas City	*417*	*22*	*888*	*204*
Denver	*107*	*1*	*732*	*195*
Huntsville	*46*	*3*	*175*	*313*

8.1.2 Conclusions

A few points can be made here with regard to incorporating a discriminant capability into the rotation algorithm. One is the importance of acquiring training data for the site where the system will be run, as was seen with the parameter tuning. Results from a site that is meteorologically similar could also be used. It should also be noted that although the implementation of the discriminant function may be useful, it may also be computationally expensive for use in a real-time system. The calculation to be used according to this analysis involves the multiplication of a 5 X 5 matrix with two vectors, for a total of at least 122 operations to be performed for the classification of each detection. Whether this can be performed quickly enough in real time is a function of the computer system used.

It is more significant that the final results agree with the parameter tuning approach in that the number of segments in a rotation region figures strongly in its chances of being a successful detection. Another ramification of this result, however, is that the number of segments is also a feature that can vary greatly with the geographical source of the data, and is the most discriminating feature found in the analysis. Since this technique requires training data before the algorithm can be made operational, it is necessary to generate truth for every proposed site where the algorithm will be used. If this practical consideration cannot be accommodated, then adding a discriminant capability to the rotation algorithm would not be worthwhile.

9. SUMMARY AND CONCLUSIONS

Tests show that parameter tuning can dramatically alter the performance of the rotation algorithm. Although the algorithm thresholds chosen to be varied made theoretical and meteorological sense, sometimes they did not seem to have much impact unless testing results were separated by site. It is important, therefore, that parameter testing be done on a homogeneous set of test data, that is, all from the same meteorologically similar region, in order to obtain appropriate parameter settings. This is evident because various algorithm sensitivities, such as the presence of strong environmental winds or low signal-to-noise ratios, are indigenous to particular geographical areas. Although this data segregation is critical to achieving maximum algorithm performance, for experimental reasons the data used for this study was a mixture of three sites. Nevertheless, the results were a detection probability of 84 percent and a false detection rate of 37 percent for the higher reflectivity regions. Tests on a smaller statistical scale point strongly toward a much higher POD (up to 100 percent) and lower PFD (as low as 17 percent) when algorithm parameter adjustments are made with regard to the particularities of a radar site. Furthermore, the logic and parameter changes made to the algorithm resulted in a lower detections-to-truth ratio, signifying improvement to the discretion of the algorithm's decision-making process.

The major focus of the algorithm improvement process was to decrease its false detection rate, and this was successful. Without benefit of reflectivity or storm cell information, though the algorithm can always detect azimuthal shear; it may not necessarily be a rotation region associated with a microburst. Thus, the PFD can be lowered a limited amount.

The results of a preliminary discriminant analysis show that if the discriminant function were to be included in the algorithm's implementation, 27 percent of the number of false detections would be eliminated while the number of valid regions lost would represent only seven percent of the POD. The analysis showed that the number of segments in a region is its most distinguishing characteristic, although other features, such as shear, area and velocity differential should be included in the covariance matrix calculation.

The main conclusion is that segments should be allowed to be shorter and more numerous, while at the same time the azimuthal association criteria should be loosened. In this way, spurious segments will be grouped together into regions that ultimately will be invalidated because of insufficient area, while legitimate rotation will be detectable, even though the data may be noisy.

9.1 RECOMMENDATIONS

The shear validation test with its **shear_drop** threshold was successful in helping to reduce the PFD overall, and it should be included in the next release of the rotation algorithm. Furthermore, parameter tuning should be done after testing has been done on data from that meteorological region only. Data from different sites should not be combined when running tests for threshold adjustments. The final parameter set determined by this study is superior to the currently operational one, and it represents a good starting point.

The technique used for parameter optimization was basically heuristic, and it worked well for the set of parameters used because intimate knowledge of the algorithm's behavior could be employed as the the parameters were adjusted. An alternative technique would be to organize the various measures of algorithm performance into a function and then maximize this function in n-space (where n is the number of relevant parameters to be adjusted) using a gradient method. The disadvantage of this method is that it may be impractical, requiring too many iterations of running the algorithm and grading its performance on large data set.

Discriminant analysis can be directly useful for significant false detection rate reduction if incorporated into the algorithm. It also can be indirectly useful for close inspection of characteristics of algorithm output, which can provide information on further improvements to the POD.

Dual Doppler analysis would also be helpful in the characterization of a valid rotation region. The dual Doppler windfield could be compared to the single Doppler image, which could provide some insight on how to interpret the rotation image, resulting in further reduction of the algorithm's PFD.

If the effects of strong environmental winds could be filtered out of the radar image, the rotation algorithm could then be made to search for velocity runs of negative to positive (and positive to negative), as opposed to just increasing or decreasing, which then bears a closer resemblance to the canonical radar signature of rotation as depicted in Figure 4b. Though other causes of false detections would still exist, the large number due strictly to an environmental wind effect could be reduced.

More research is needed to arrive at an optimum value for the **shear_drop** threshold. It may be possible to use simulated data to quantify the second derivative changes in the sine-like function of the model signature to get the proper value. However, a good statistical sampling of data for the site in question may be a better alternative.

If the data for entire scan can be stored and retrieved efficiently in real-time, then the pattern matching process of the rotation algorithm can be extended to two dimensions. Since far more research in general has been done on two-dimensional images, this opens up many possibilities for using more well-known and stable image processing techniques, such as a two-dimensional matched filter. Furthermore, one would then be able to take advantage of available reflectivity information, assuming it could also be processed for an entire scan.

Investigation into the use of the spectrum width product of the radar may be fruitful. This has a good possibility of success because of the high variance of velocities in most rotation regions in the vicinity of downdrafts.

GLOSSARY

TDWR	Terminal Doppler Weather Radar
PRF	Pulse Repetition Frequency
isodop	A line connecting points of the same Doppler velocity.
bounding boxes	Axis aligned polygon formed by connecting the four coordinates (x min, y min, x max, y max) which give the x–y extrema of a region.
shear segments	Lines connecting points of increasing or decreasing velocity.
AGL	Above Ground Level
truth (ground truth)	Regions of interest as determined by a human expert.
PFD	Probability of False Detection
POD	Probability of Detection
DTR	Detection–to–Truth Ratio
ASP	Automatic Scoring Program
RR	Event Recognition Rate
event	A group of truth observations occurring over time within the life span of a microburst.
SNR	Signal–to–Noise Ratio
wet	High reflectivity (above 45 dbZ)
dry	Low reflectivity (15 dbZ)

REFERENCES

1. S.D. Campbell, and M.A. Isaminger, "A prototype microburst prediction product for the Terminal Doppler Weather Radar," *16th Conference on Severe Local Storms,* Kananaskis Provincial Park, Alberta, Canada, Oct. 22–26 (1990).

2. M.W. Merritt, D. Klingle-Wilson, and S.D. Campbell, "Wind shear detection with pencil-beam radars," *The Lincoln Laboratory Journal*, 2, 483–510 (1989).

3. S.D. Campbell, "Use of features aloft in the TDWR microburst recognition algorithm," *24th Conference on Radar Meteorology,* Tallahassee, FL, March, (1989).

4. S.C. Crocker, "TDWR PRF selection criteria," M.I.T. Lincoln Laboratory, Lexington, MA, Project Report ATC-144, Revision 1, FAA Technical Report DOT/FAA/PM-87-25 (1988).

5. S.D. Campbell, and M.W. Merritt, "TDWR scan strategy requirements, revision 1," M.I.T. Lincoln Laboratory, Lexington, MA, Project Report ATC-144, Revision 1, FAA Technical Report DOT/FAA/PM-87-22 (1990).

6. D.S. Zrnic, D.W. Burgess, and L.D. Hennington, "Automatic detection of mesocyclonic shear with Doppler radar," *Journal of Atmospheric and Oceanic Technology*, 2, (1985).

7. V.T. Wood, and R.A. Brown, "Single Doppler velocity signatures: an atlas of patterns in clear air/widespread precipitation and convective storms," National Severe Storms Laboratory, Norman, OK, NOAA Technical Memorandum ERL NSSL-95, p.26, (1983).

8. M.A. Isaminger, (personal communication, May 8, 1990).

9. P.J. Biron, and M.A. Isaminger, "Analysis of microburst characteristics related to automatic detection from Huntsville, AL and Denver, CO," *24th Conference on Radar Meteorology,* Tallahassee, FL, March (1989).

10. J. Stillson, (personal communication, June 25, 1990).

APPENDIX A:

SYNOPTIC SUMMARIES

The following tables list the characteristics of all the microburst events on each case date in this study. Note that in all the following tables, the reflectivity is the value of the core reflectivity at the surface.

July 25, 1986, Huntsville, AL -- Seven high-reflectivity microbursts and one gust front occurred on this day, which was hot with characteristic air-mass thundershowers.

Microburst Characteristics

Time (CDT)	Location Rng/Az	Intensity m/s	Reflectivity dbZ
1354	25/184	15	55
1519	21/251	12	55
1519	27/253	12	n/a
2004	20/215	21	55
2040	20/142	21	55
2148	4/124	27	60
2206	23/075	21	55

September 2, 1987 Denver, CO -- There were 11 microbursts and four gust fronts on this day, which was warm with thundershowers. By noon, a line of thundershowers extend along the front range [of the Rocky Mountains]. Several microburst scale outflows were detected over the mountains. At 1250 MDT a gust front was scanned west of Stapleton International Airport in Denver. A weak divergent line had developed by 1300 MDT (see below).

Microburst Characteristics

Time (CDT)	Location Rng/Az	Intensity m/s	Reflectivity dbZ
1123	61/245	16	40
1233	42/261	18	40
1255	24/266	12	15
1304	30/249	12	10
1616	26/305	24	20
1630	31/016	15	60
1649	23/309	24	20
1659	6/322	18	15
1703	9/356	21	20
1745	27/057	24	40
1751	33/042	24	25

July 1, 1989, Kansas City, MO -- On this day, there were eight microbursts and one gust front. The combination of a vorticity lobe and low-level moisture in the Kansas City area touched off thundershowers during the mid-afternoon hours. By 2230, several weak to moderate microbursts were detected to the northeast and southeast of the radar. A weak microburst at 2215 set off a wind shear alert at the airport.

Microburst Characteristics

Time (CDT)	Location Rng/Az	Intensity m/s	Reflectivity dbZ
1959	26/037	19	54
2009	26/141	10	40
2050	6/092	11	45
2100	22/076	16	45
2117	30/076	10	n/a
2145	16/067	10	45
2215	13/040	11	45
2224	20/190	10	n/a

July 30, 1989, Kansas City, MO -- The day was warm with thundershowers, and there were 19 microbursts and three gust fronts. An abundant supply of moisture and an outflow boundary from central Missouri combined to produce moderate to severe thunderstorms in the Kansas City area during the early morning hours. Several moderate to strong microbursts were observed to the east and northeast during this time. At 0930 UT, the "Claycomo" microburst, with a total shear of 40 m/s, was observed at 29/093. This microburst downed several large trees and damaged several trailer homes.

Microburst Characteristics

Time (CDT)	Location Rng/Az	Intensity m/s	Reflectivity dbZ
0710	15/110	30	40
0723	17/103	21	35
0727	26/084	24	40
0734	22/107	12	40
0736	32/072	15	42
0742	20/110	15	40
0751	29/100	11	40
0757	24/021	16	35
0818	23/051	11	35
0851	22/075	10	35
0859	20/099	12	43
0908	24/073	12	30
0914	23/098	14	42
0927	25/103	10	40
0928	28/092	40	45
0930	23/084	15	30
0941	23/088	12	40
0947	30/102	15	40
0946	23/087	10	40